Available online at www.sciencedirect.com
ScienceDirect
Journal of Nuclear Materials 372 (2008) 318–339
journal of nuclear materials
www.elsevier.com/locate/jnucmat

Detailed characterisations of high burn-up structures in oxide fuels

J. Noirot *, L. Desgranges, J. Lamontagne

Commissariat à l'Energie Atomique (CEA) Cadarache, 13108 St. Paul Lez Durance, France

Received 6 February 2007; accepted 2 April 2007

Abstract

In this paper, a series of post-irradiation examination results on high burn-up structures (HBS) are summarised for a wide variety of fuels (various programmes on PWR UO_2 fuels with different claddings and with or without doping, PWR MOX fuels, FBR fuels, etc.). This summary is intended to provide a better understanding of how high burn-up structure is formed and subsequently changes up to very high burn-ups in various irradiation conditions. This paper also focuses on the existence of planar defects prior to the HBS formation and their change with time, as well as on the chemical influences and consequences of the HBS. Two new mechanisms are proposed to take into account these observations.

PACS: 28.41.Bm; 81.05.Je

1. Introduction

With the current increase in target fuel burn-ups for LWRs and the irradiation of precursor fuels at even higher burn-ups, research has focused on the formation of a porous, small-grained microstructure in the rim area of the fuel, first called 'rim' structure before being called high burn-up structure (HBS). Many teams have looked into this phenomenon, each helping to characterise and understand the properties of this new material. Some programmes were even totally devoted to this subject [1].

So far, CEA hot laboratories have contributed various elements to this research, especially.

Providing a first example of high burn-up fuel exhibiting this microstructure in the rim area [2].

Demonstrating the presence of two types of sub-grains in the HBS; round around the bubbles, and polyhedral elsewhere [3]. It also gave porosity values, discussed the nature of planar defects observed near HBS areas to conclude that such defects might play a role in the formation of polyhedral sub-grains or bubbles.

Showing that the rim area may contribute to the overall fission gas release in the free volumes of the rods [4] , but above all showing that such release did not exceed 0.3% of the formed gas when the mean rod burn-up was 60 GWd/t, i.e., local release in the rim area not exceeding 5%. Releases from this area are therefore insufficient to explain the increase in the fission gas release rate measured at high burn-up.

Finally, studies [5–7] have provided further information especially with an assessment of the quantity of fission gas in a single bubble in the rim area and the confirmation of low fission gas release from this area by secondary ion mass spectrometer (SIMS).

In spite of considerable research already performed on this subject all over the world, it seems that this phenomenon is not fully understood and that consensus has not been reached.

This paper provides a summary of numerous observations on HBS in various fuels (programmes on PWR UO_2 fuels with different claddings and with or without doping, MIMAS PWR MOX fuels, FBR fuels, etc.). Observations were made using optical microscopy, an electron probe microanalyser (EPMA), a scanning electron microscope (SEM) and a secondary ion mass spectrometer

* Corresponding author. Tel.: +33 442254497; fax: +33 442253611.
E-mail address: jean.noirot@cea.fr (J. Noirot).

0022-3115/$ - see front matter © 2007 Published by Elsevier B.V.
doi:10.1016/j.jnucmat.2007.04.037

(SIMS). These results provide new information on the conditions resulting in the formation of HBS, on HBS properties and on the changes of HBS during irradiation. These results put HBS in a new light.

2. Fuel data

Table 1 lists the main features of the fuel families on which various examinations in this study were based.

Apart from tiny manufacturing differences, the main difference between fuels (**1**) and (**2**) lies in the ^{235}U enrichment, which was 3.7 for (**1**) and 4.5 for (**2**). The main difference between (**2**) and (**3**) was the cladding: Zircaloy 4 for (**2**) and M5™ for (**3**).

Fuels (**4**) were MOX fuels manufactured according to the MIMAS process [8,9]. This MIMAS process leads to microstructures composed of:

- Plutonium-rich agglomerates with a Pu content close to that of the master blend, i.e., less than 30%.
- Uranium-rich agglomerates with very low plutonium content.
- A matrix coating these two phases with an intermediate Pu content.

The great interest in examining MOX fuel to study the formation and subsequent changes of HBS lies in the very broad range of local burn-ups that can be found in the Pu-rich agglomerates (up to 270 GWd/t in this study) and in the wide range of temperatures occurring in these agglomerates depending on the radial position during the same irradiation.

Fuels (**5**) had additives introduced during fabrication in order to (a) increase the fuel grain size during pellet sintering, (b) form precipitates to help the fission gases precipitate into intragranular bubbles, and (c) modify the mechanical properties of the pellets [10]. These microstructures were designed to improve the fuel behaviour in terms of pellet–cladding interactions (PCI) and have been successfully tested [11,12]. The fuels in this experiment and standard UO_2 mainly differ by their pellet geometry, the ^{235}U fuel enrichment, and the irradiation conditions. In the Tanoxos (**5**) experiment, the pellet diameter was only 4.93 mm and irradiation in the Osiris experimental reactor led to high burn-up in less than two years of irradiation, but with low powers and temperatures during the last part of the irradiation. Moreover, stainless steel cladding and extra external aluminium cladding induced a high stress level in the fuel after gap closure.

Fuels (**6**) are examples of fast breeder reactor fuels irradiated in the Phenix reactor.

3. Experimental methods

For the purpose of observations, the samples were prepared by (a) fracturing the fuel to examine the surface with a SEM, or (b) grinding and polishing the cross sections or longitudinal sections. Great care is necessary to correctly prepare the HBS, especially during the last steps of the polishing. As HBS are constituted of grains with diameters that can be 0.15 μm only, the sample surface cannot be considered correct unless the polishing granulometry is gradually decreased to 0.25 μm for diamond pastes. At last, a final step using a colloidal solution of silica (0.04 μm) greatly improves the result.

The examinations used in this study were conducted in the hot cells of the CEA LECA-STAR facility at Cadarache (France) with:

- An Olympus PME3 optical microscope for which hot cell adaptations were done with the help of 'Optique Peters'. The image acquisition was composed of an F-View II camera on the 'SIS' acquisition system from which the AnalySIS software was also used for image analysis.
- A shielded electronic microprobe (EPMA) Camebax microbeam from 'CAMECA' equipped for acquisition and exploitation of the measurements using the 'SAMx' system.
- A scanning electron microscope (SEM) 'Philips' XL30 on which the WDX 'Microspec' spectrometer has 'home made' shielding. Large field acquisitions were performed thanks to the ADDA 'SIS' system, with the AnalySIS software once again used for image analysis.
- A secondary ion mass spectrometer (SIMS) 'CAMECA' IMS 6f capable of analysing the same samples as the SEM and EPMA.

Table 1
Main data on fuels used in this study

Name (in this study)	Fuel type	Mean burn-up range of sample	Cladding	^{235}U enrichment or Pu content	As-fabricated grain sizes
(**1**) UO_2–Zr4	UO_2 standard PWR geometry	Up to 62 GWd/t	Zr4	3.7% ^{235}U	~9 μm
(**2**) UO_2–Zr4	UO_2 standard PWR geometry	Up to 68 GWd/t	Zr4	4.5%^{235}U	~11 μm
(**3**) UO_2–M5™	UO_2 standard PWR geometry	Up to 78 GWd/t	M5™	4.5%^{235}U	~11 μm
(**4**) MOX MIMAS	MIMAS MOX standard PWR geometry	Up to 63 GWd/t	Zr4	6%Pu/(U + Pu)	~7 μm
(**5**) Tanoxos	Advanced and standard microstructure in the Osiris research reactor	65 GWd/t	Stainless steel + Al	7%^{235}U	9 μm and 75 μm
(**6**) FBR	FBR fuel irradiated in Phenix reactor	Up to 17%FIMA	Stainless steels	~20%Pu/(U + Pu)	~10 μm

4. Results

4.1. Formation of high burn-up structures (HBS)

4.1.1. What is a high burn-up structure?

When fully developed, an HBS exhibits very small grains and large bubbles instead of the as-sintered initial grains. The bubbles are surrounded by round sub-grains whereas the rest is made of polyhedral sub-grains. In the case of MOX (Fig. 1(b)), the limit of the fully developed HBS is clear. In the case of UO_2 (Fig. 1(a)), the existence of fully developed areas is clear, but their limit remains unclear. Outside of these fully developed HBS areas, isolated sets of bubbles and sub-grains can be found in almost intact initial grains. Each stage of the HBS development exists between these two phases, including areas where only small parts of the initial grains are still intact.

On optical ceramographs of a polished sample, the HBS first appears through its porosity. After chemical etching designed to reveal the grain boundaries, the HBS areas may show little grains or appear very dark if the etching was overly efficient. In the HBS, a large part of the fission gas leaves the bulk of the oxide to form bubbles. On the observation plane, bubbles have released their gas, having been opened by polishing. As a consequence, in spite of the high amount of fission gases still inside the HBS, the EPMA measurements or maps on the xenon give low values, except in a few spots when bubbles are very close to the surface.

4.1.2. Before the high burn-up structure: planar defects

To our knowledge, Pati was the first to point out the existence of 'needle-shaped features' in the nuclear fuel at high burn-up [13]. He suggested that it could be U_4O_9. The nature of these defects was discussed in [3] and linked to the planar defects observed with TEM [14,15]. It was then suggested that these defects could form the boundaries of the polyhedral sub-grains.

Since then, planar defects have systematically been observed after chemical etching of polished samples, both around HBS areas and in the highest fuel burn-up locations yet to undergo restructuring, always in the cold regions of the fuel. For example, such defects are detected:

- At intermediate burn-up (~30 to 40 GWd/t) on the periphery of UO_2 fuels. As an example, Fig. 2 shows a (**3**) type fuel UO_2–M5™, irradiated 5 cycles up to a mean rod burn-up of 56 GWd/t. However, the fuel was located close to the bottom of the rod at a position where the local burn-up was only 30 GWd/t. It shows a very high level of planar defects. The particularities of this position were the low fission rate and the low temperature.
- Around the HBS of the peripheral plutonium-rich agglomerates in the MIMAS MOX fuels (**4**) as in Fig. 3 on the periphery of a fuel at 57 GWd/t.
- Beyond the limits of the rim areas of UO_2 fuels (**1**), (**2**) and (**3**) as in Fig. 4 on a 69 GWd/t (**3**) UO_2–M5™ fuel. In this case, they were mixed with isolated HBS areas.

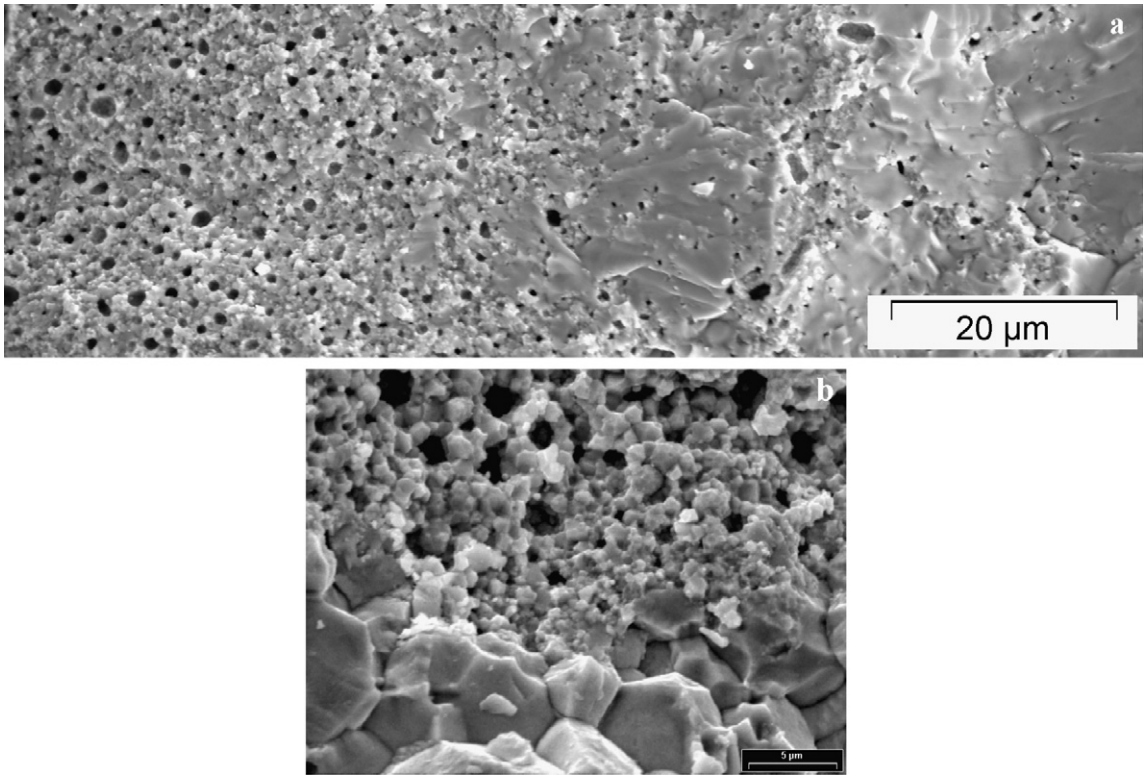

Fig. 1. SEM fractographs illustrating a HBS (a) at the rim of a UO_2–M5™ (**3**) 73 GWd/t pellet and (b) in a 55 GWd/t MOX MIMAS (**4**) fuel.

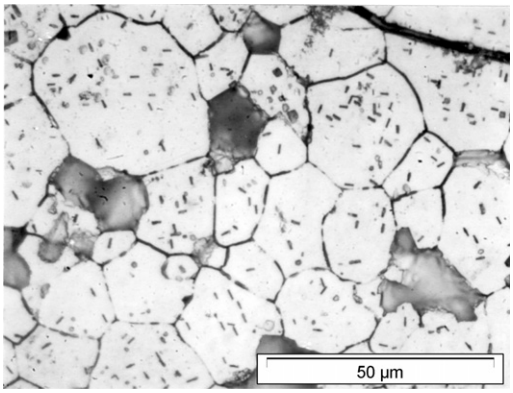

Fig. 2. Optical ceramograph after chemical etching of a 30 GWd/t (**3**) UO_2–M5™ fuel.

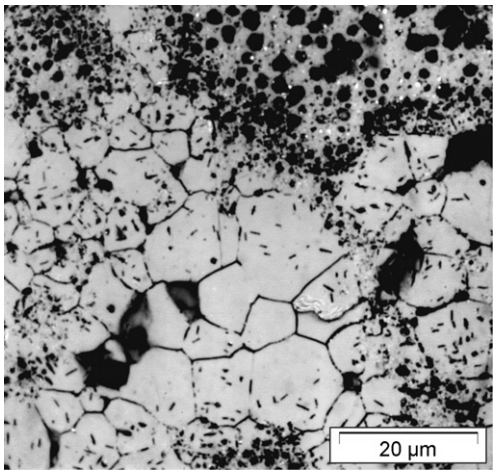

Fig. 3. Planar defects observed by optical microscopy at the periphery of a 57 GWd/t (**4**) MOX MIMAS sample after chemical etching. These defects are found in the UO_2 zones around Pu-rich agglomerates.

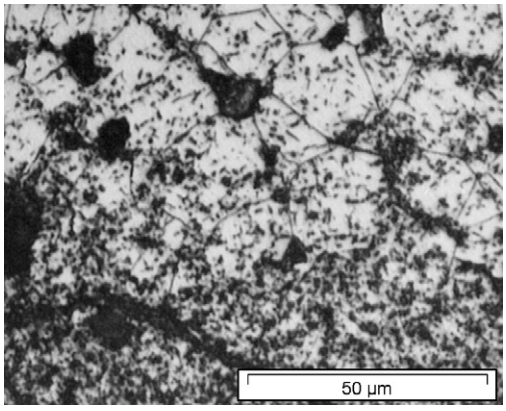

Fig. 4. Planar defects observed by optical microscopy at the back of the rim zone of a 69 GWd/t (**3**) UO_2–M5™ fuel after chemical etching.

Planar defects cannot be found in the fully developed HBS itself or around the central MOX plutonium agglomerates.

Because of the high increase in the burn-up of the MOX plutonium agglomerates during one cycle, we had no opportunity to observe these agglomerates slightly before the HBS formation. We therefore cannot be sure such planar defects exist in this case.

Moreover, defects can be observed without any etching on SEM fractographs, showing that they are not an effect of the sample preparation (etching or TEM sample preparation). In these fractographs, the defects appear as steps of about 1 μm long on the fractured surface (Fig. 5), which implies a structural discontinuity at the position of the planar defects. Dedicated EPMA X-ray maps of xenon or metallic fission products in areas where planar defects have been detected by optical microscopy do not make it possible to reveal any local decrease or increase in the content of these fission products.

After reactivity-induced accident (RIA) tests [16], ramp tests, or annealing tests [17], the length of these defects increases and some of them can be seen on polished samples, even without chemical etching.

Some fractographic observations also show that part of the planar defects (perhaps the older defects) exhibit a rounded grain microstructure at their surface that seems similar to what is usually observed around HBS bubbles (Figs. 5(c) and 6). Moreover, the lips of the defects tend to open.

During the HBS formation process, the planar defects are the first to appear. They then evolve into bubbles. Round sub-grains form on the surfaces of the planar defects at the periphery. However, it seems that the round sub-grains cannot be clearly distinguished during the HBS initiation far from the periphery. The polyhedral sub-grains are formed later, from the remnants of the initial grains, when the number of bubbles and round sub-grains is high.

4.1.3. The main driving force leading to the HBS formation is not the fission itself but the implantation of the fission products

In MIMAS MOX fuels (**4**), fissions occurring in the Pu-rich agglomerates of course lead to much higher fission product contents than those observed in the rest of the pellet. Nevertheless, as part of these fission products are implanted all around these Pu-rich agglomerates, the periphery of these agglomerates and their immediate neighbourhood exhibit intermediate contents of fission products, decreasing from the central part of the agglomerates outwards (matrix coating the agglomerates and uranium-rich agglomerates). Due to this high implantation of fission products and in spite of the local burn-up that is actually low, HBS is formed beyond the limits of the Pu-rich agglomerates. Fig. 7 illustrates this observation on a MOX MIMAS (**4**) fuel, in an area located between 30 and 100 μm from the pellet edge. The mean fuel burn-up at this level was 57 GWd/t, but a burn-up of about 180 GWd/t was reached in these agglomerates whereas it

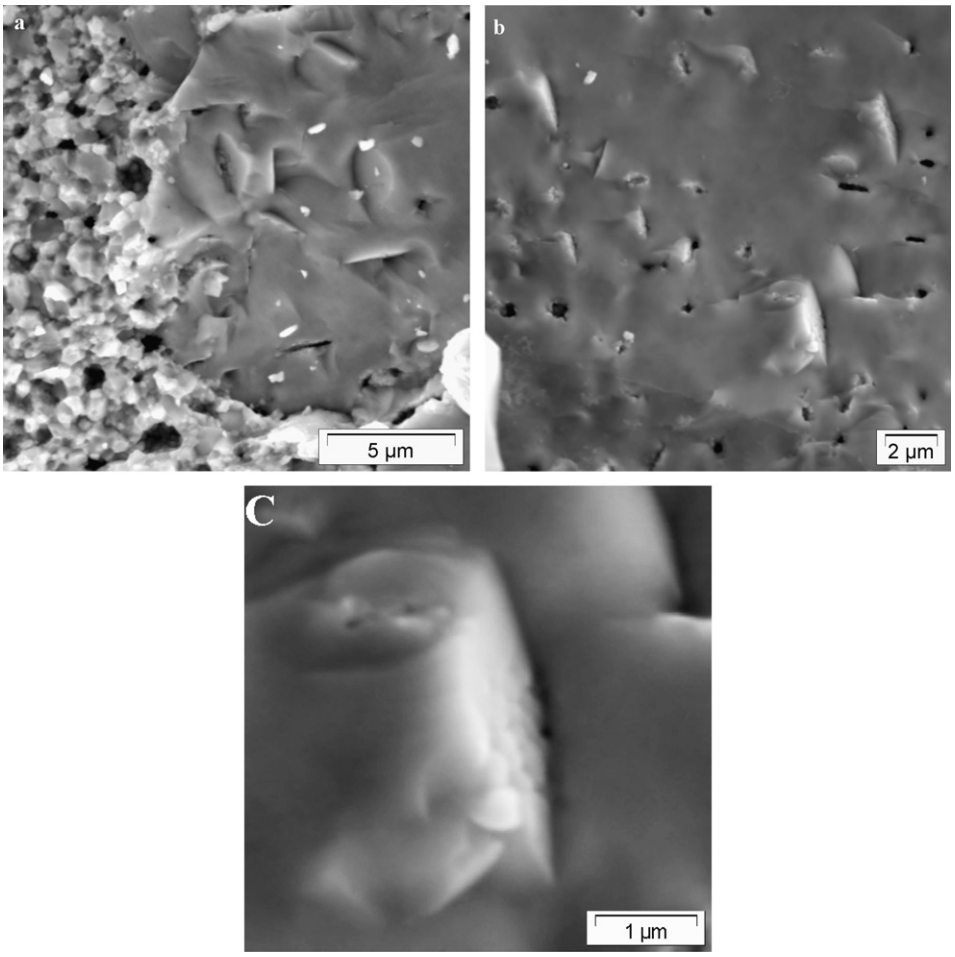

Fig. 5. SEM fractographs showing planar defects without chemical etching on a 57 GWd/t (**4**) MOX MIMAS fuel (a) and a 72 GWd/t (**3**) UO_2–M5™ fuel (b) with a detail (c).

was only about 50 GWd/t around the agglomerates. The EPMA plutonium X-ray mapping made it possible to position the limits of the Pu-rich agglomerates. This limit is superimposed on the SEM image, the neodymium X-ray map and the xenon X-ray map. The positions of the bubbles and the low xenon measurement areas on the X-ray map show the extent of the HBS outside the limits of the agglomerates.

In the MIMAS MOX fuel case, a reverse phenomenon occurs when the Pu-rich agglomerate is small. In this case, most of the fission products are implanted outside the agglomerate. The amount of fission products found in this little agglomerate is therefore much lower than that in the centre of the large agglomerates. It is thus possible to find small agglomerates with no HBS though the large agglomerates in the same area have this HBS form, with an identical actual burn-up. This is particularly the case for the smallest agglomerates shown in Fig. 12.

4.1.4. Effect of temperature on the formation of HBS

Studying the formation of HBS in MIMAS MOX fuels (**4**) makes it possible to examine the effect of temperature on the microstructure resulting from restructuring. On a single cross section, apart from the outer periphery agglomerates, all Pu-rich agglomerates more or less undergo the same power history and hence the same fission rates. However, the temperature is a function of the radial position.

Measurements of the size of the bubbles and the subgrains in the HBS of large Pu-rich agglomerates show that both sizes increase with temperature.

Fig. 8 shows grain and bubble sizes measured in the Pu-rich agglomerates of a MIMAS MOX (**4**) fuel, as a function of the distance from the periphery, i.e., the variation in these sizes with the irradiation temperatures.

These measurements were performed using SEM fractography. They are average values of punctual measurements: there is a wide range of sizes in both the bubbles and the grains for each agglomerate. Nevertheless, these values show the kind of increase that is always observed in MOX fuel agglomerates by fractography or by optical ceramography after etching.

Concerning the extreme periphery, the higher burn-up observed in the agglomerates tends to induce the existence of bigger bubbles, which is discussed in Section 4.3.2. Fig. 8 only shows the changes of bubbles and grains sizes between the periphery and the mid-radius. While the peripheral

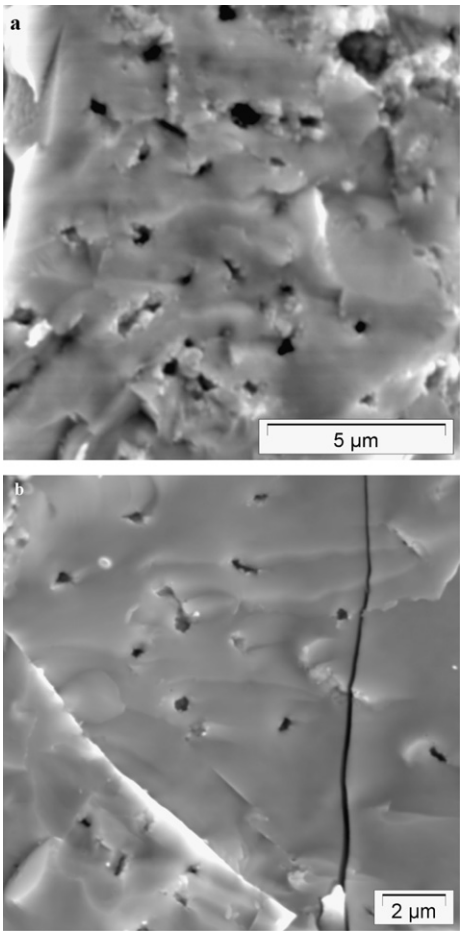

Fig. 6. Opening of the planar defects with round sub-grains at their surfaces in SEM fractographs of 61 (a) and 73 (b) GWd/t (**3**) UO_2–M5™ samples.

agglomerates undergo the classical HBS formation, the hot central part of the pellet agglomerates undergoes huge transformations with the appearance of very large bubbles, though the grains sizes remain very similar to the initial sizes but with shape modifications. Fig. 9 shows the bubbles in large Pu-rich agglomerates at 0.9R, 0.5R and close to the centre for a 45 GWd/t MIMAS MOX (**4**) sample. The increase in the size of the bubbles and the grains around mid-radius is very sharp.

It is commonly admitted that the formation of an HBS is the result of the balance between the formation of defects due to irradiation, and the thermal annealing of these defects. At the very least, a threshold temperature seems to exist, above which the high burn-up changes do not lead to the formation of small grains.

If such a balance exists, the following can be expected on a local level:

– fuel that does not have a high burn-up in spite of high local burn-up, and
– fuel that has a high burn-up structure at the same local burn-up and temperature range owing to a higher fission rate.

This kind of comparison should be possible in intermediate areas where the temperature is slightly below the threshold temperature in such a way that some annealing of the formed defects can be expected. The best way to look for such effects is most likely a comparison between:

– a low burn-up MOX fuel in a mid-radius agglomerate (which has just become HBS with a high fission rate) and,
– another MOX fuel at a higher mean burn-up, focusing on the intermediate Pu content phase so that the local content of the fission products is the same as the previous one.

All comparisons of this kind revealed HBS in both cases. The only point that may show this temperature effect is, in case of MIMAS fuels where there is very little intermediate Pu content matrix, the fact that the HBS does not develop beyond the limits of the Pu-rich agglomerates when these agglomerates are not at the pellet periphery (Fig. 10). Nevertheless, other parameters may also affect the formation of the HBS, especially the stress field and the local plutonium content outside the agglomerates, which is lower in this case (see Section 4.1.6).

4.1.5. Role of initial grain boundaries

In [18], resistance to the formation of HBS in two types of large grain pellets (undoped and alumino-silicate doped) is reported. An explanation designates the grain boundaries as the initial sites responsible for the formation of the HBS.

However, the formation of the HBS does not especially start at the grain boundaries. Fig. 11 shows a SEM image of a (**2**) UO_2–Zr4 sample irradiated up to a mean burn-up of 45 GWd/t in which the formation of the HBS in the rim is new.

The contrasts have been enhanced so that the channeling effects on the electrons show the differences in the grain orientations, and hence the position of most of the grain boundaries. To a large degree, the initial grain structures remained intact in this fuel, in spite of the fact that the HBS has begun to form. It also appears that most of the HBS bubbles had an intragranular position and that the grain boundaries played no role in their formation.

4.1.6. Possible role of plutonium content in the formation of HBS

Evidence of an effect of a high plutonium content upon the formation of an HBS lies in both the absence of bubble formation and the high implanted xenon content measured by EPMA in UO_2 grains that can sometimes be very close or even included in Pu-rich agglomerates of MOX fuel (**4**).

Examples of such effects on two large Pu-rich agglomerates in two MOX MIMAS fuels (**4**), respectively, irradiated up to mean cross section burn-ups of 26 GWd/t and 58 GWd/t, are shown in Figs. 12 and 13. In these two cases,

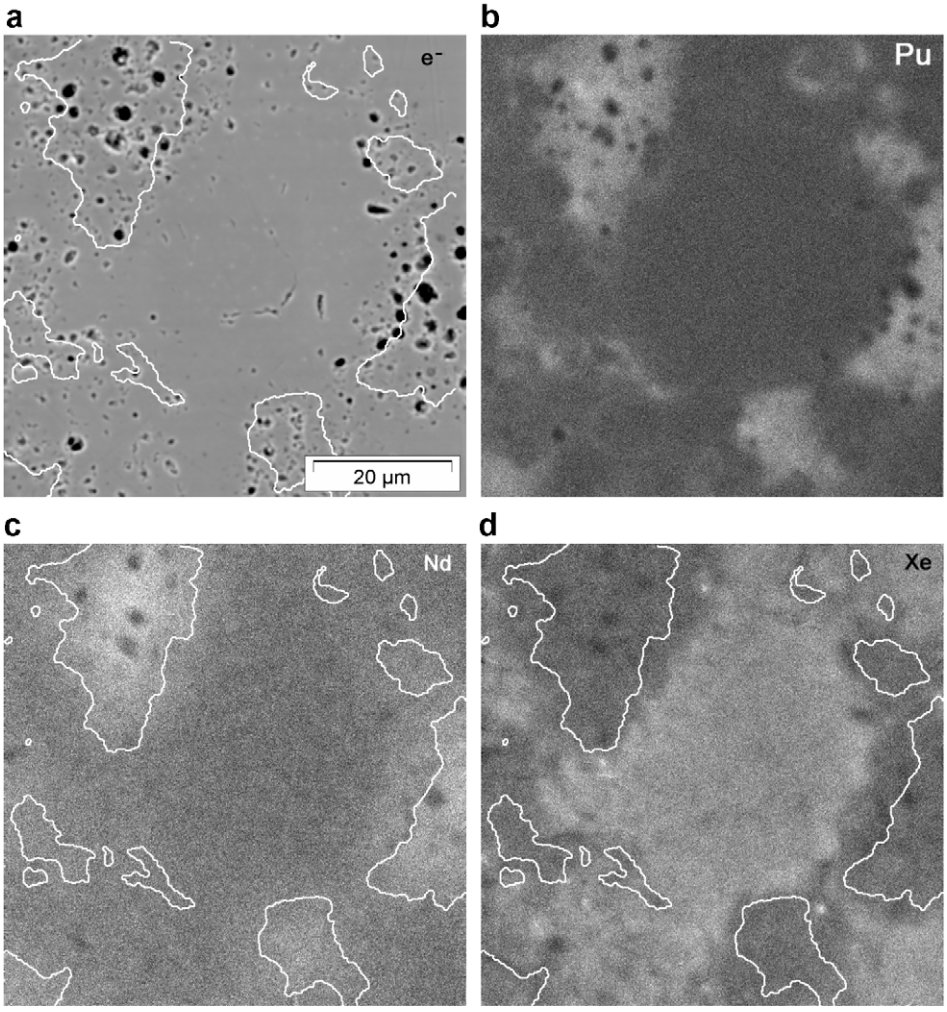

Fig. 7. SEM and EPMA X-ray maps on MIMAS MOX (**4**). These images show the relative position of limits of the plutonium-enriched agglomerates and the HBS. The burn-up reaches 180 GWd/t in these peripheral agglomerates. They show the extent of the HBS beyond the limits of the Pu-rich agglomerates.

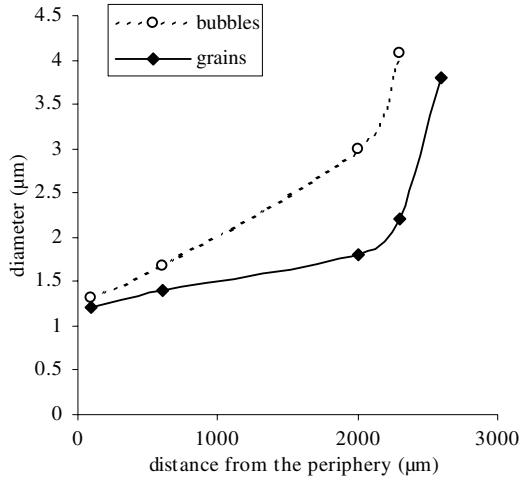

Fig. 8. Mean sizes of bubbles and grains in the HBS of Pu agglomerates in a 45 GWd/t MIMAS MOX (**4**) fuel.

restructuring into HBS did not occur in parts of the fuel where the neodymium content was higher than in other places where restructuring occurred. The difference between these two parts of the fuel was the plutonium content, which remained low in the unrestructured parts. The limits of these areas were the same as the limits of the as-fabricated Pu-free grains. Because of this absence of restructuration, the xenon measured in these unrestructured grains was higher than the maximum values usually found in nuclear fuels [19]. This is particularly true in Fig. 13 where a xenon wt% of 1.4% was reached without restructuring. This corresponds to the concentration found in 100 GWd/t fuels.

If such an effect exists, it can only be a chemical effect of plutonium, and most probably owing to its influence on the stoichiometry. SIMS maps of irradiated MOX fuel on the UO_3^- signal indeed show stoichiometric differences between the plutonium-rich agglomerates and the rest of the pellet.

4.1.7. Fast breeder reactor fuels

In mixed-oxide fast breeder reactor (FBR) fuel (**6**), the formation of HBS also occurs on the periphery of high

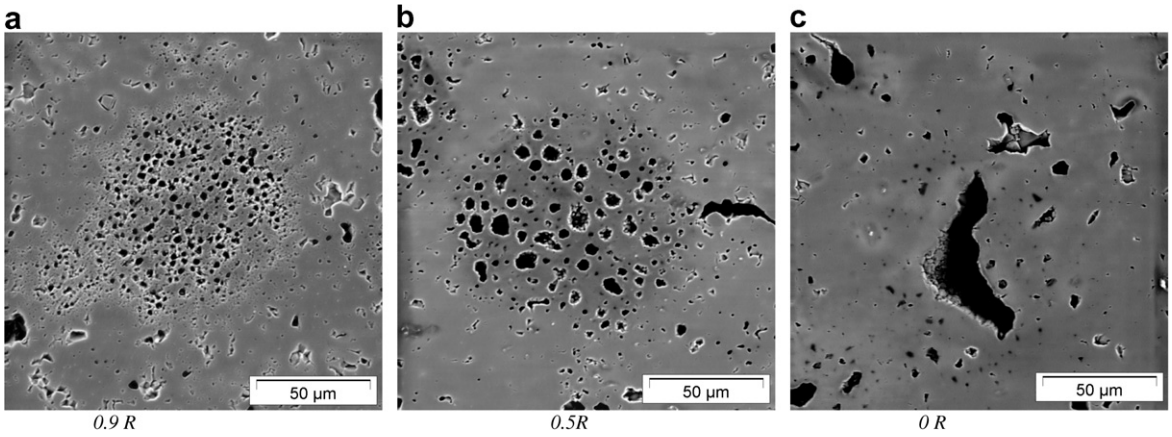

Fig. 9. Radial evolution of bubbles in the Pu agglomerate HBS for a 45 GWd/t MOX (**4**) sample (0.9R, 0.5R, centre).

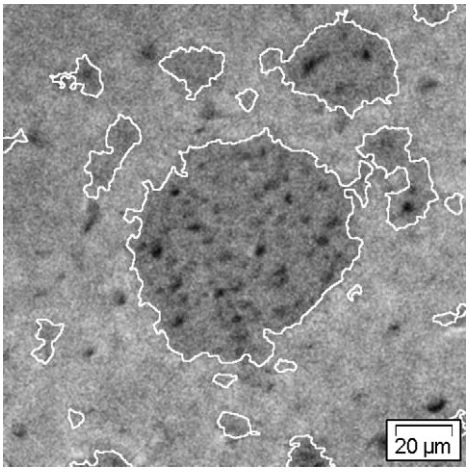

Fig. 10. EPMA Xenon X-ray map for MIMAS MOX **(4)** using the same sample as Fig. 7, but at 0.56R, showing the limits of the Pu-rich agglomerates. In this case, the HBS does not extend beyond the limits of the Pu-rich agglomerates.

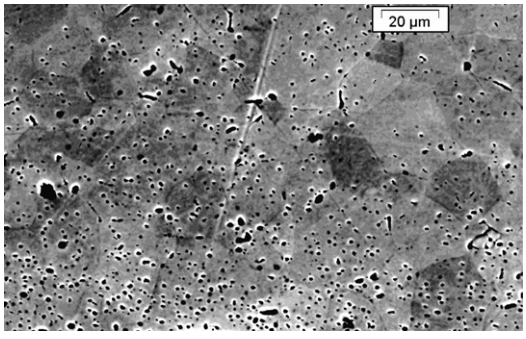

Fig. 11. SEM contrast-enhanced image of (**2**) UO_2–Zr4 45 GWd/t rim. The HBS is not developed enough for the initial grain boundaries to be erased. The HBS bubbles are mainly intragranular.

burn-up pellets. This effect is not often discussed in FBR fuel PIE articles: [20,21], but it is observed in all fuels with burn-ups greater than approximately 7% FIMA, this limit being similar to what exists in LWR fuels. This effect is observed up to the highest burn-up reached (such as in [22,23] in fuels irradiated up to 23% FIMA in the PFR reactor). In FBRs, the plutonium content is not higher on the periphery and there is no peripheral flux gradient like that found in LWRs. Nevertheless, an HBS forms in the rim of the pellets. The limitation is then due to the high temperatures reached in the central parts of the pellets. Two examples are shown in Fig. 14 with global views of the periphery and detail after chemical etching of two fuels irradiated in the Phenix reactor:

- Up to 12.5% FIMA with a low dose rate (<0.1 dpa/EFPD (equivalent full power days)) for a long time in the core (1275 EFPD): Fig. 14(a-1) and (a-2),
- Up to 17% FIMA with a 155 dpa dose for 1046 EFPD: Fig. 14(b-1) and (b-2).

Owing to the fast neutron flux, no flux dipping is observed on the periphery, which means that the burn-up in the rim area is equivalent to the mean burn-up of the sections (12.5% and 17% FIMA, i.e., ~120 and ~170 GWd/t).

In these cases, the new grains in the HBS are larger than those in the PWR UO_2 rim case, generally between 0.5 and 3 μm, but within the range of what is observed in the MIMAS MOX fuels with Pu-rich agglomerates in the hot regions. The bubbles formed can be very large (very small bubbles are observed, as are bubbles larger than 15 μm), and their shape can be far from spherical. Porosities reach 29% and 35%.

Simultaneously to the formation of the HBS in MOX FBR fuels, two other main phenomena occur:

- The formation of the '*Joint Oxide-Gaine*' JOG, a complicated association and mixture of fission products and clad corrosion products between the clad and the pellets, with a reopening of the fuel to clad gap. The JOG formation has been understood as a consequence of the evolution in the oxygen potential in relation to the burn-up, particularly influenced by the accumulation of trivalent rare earth ions [24]. The isostatic stresses in

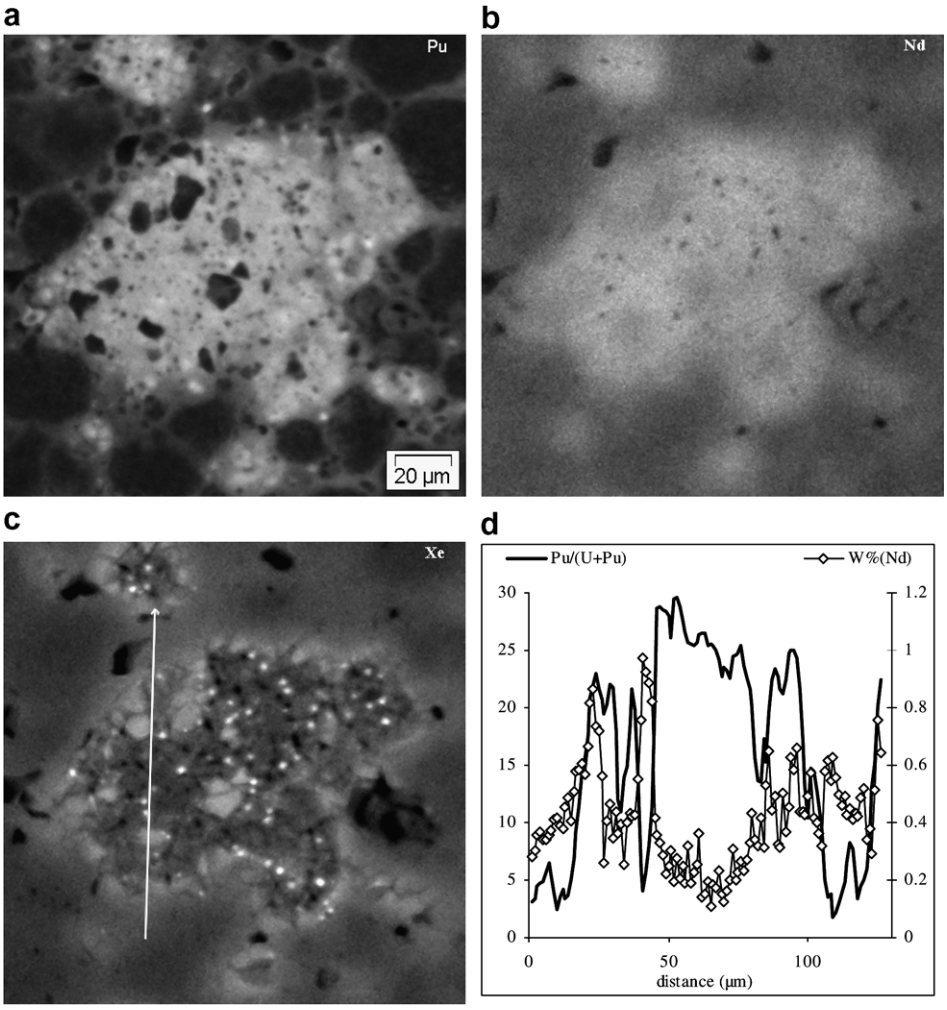

Fig. 12. EPMA X-ray maps on Pu, Nd and Xe, and quantitative analysis along a line in a (**4**) MOX MIMAS 26 GWd/t fuel. High xenon contents were measured in UO_2 grains when they were included in a Pu-rich agglomerate or very close to it. The very bright spots of the Xe X-ray map are bubbles still intact under the preparation surface in the HBS.

the fuel periphery are therefore very low during the formation of the HBS, which must affect the shape and the size of the bubbles.
- Possible corrosion of the steel clad.

These two phenomena and their implications on the overall fuel behaviour have somehow concealed the interest for the formation of HBS in these fuels.

*4.1.8. Unusual irradiation conditions may lead to unexpected features despite accumulated experience: the Tanoxos case (**5**)*

In the (**5**) Tanoxos programme [10], a standard microstructure was irradiated together with large-grain doped fuels. The design of the device led to choose stainless steel cladding with aluminium over-cladding and a small gap between the fuel and the cladding. Moreover, management of fuel rod loading times induced an irradiation with two main periods; one at standard power and the other at low power and hence at low temperature, even in the central part of the pellets.

In this case (Figs. 15 and 16), almost no defect was detectable by optical microscopy on the fuel periphery after chemical etching for both standard fuel and large-grain doped fuels. At intermediate position, numerous planar defects were observed together with a few bubbles. In the central part of the pellets, a structure very much like a HBS had formed, a 'central rim' so to speak. SEM fractography (Fig. 16) shows the bubbles surrounded by little subgrains. It seems that parts of the grains were hardly affected by restructuring, perhaps stabilised by high stresses occurring in these fuels because of the irradiation design. The selected detail shows the position of an initial grain boundary.

Too many parameters differed from the standard case to clearly understand why restructuring occurred in the pellet centre and not in the rim. The main differences are:

- The very low temperatures during half of the irradiation, with temperatures lower than 500 K on the periphery (is there a low temperature limit for the formation of HBS?) and temperatures of about 800 K at the centre.

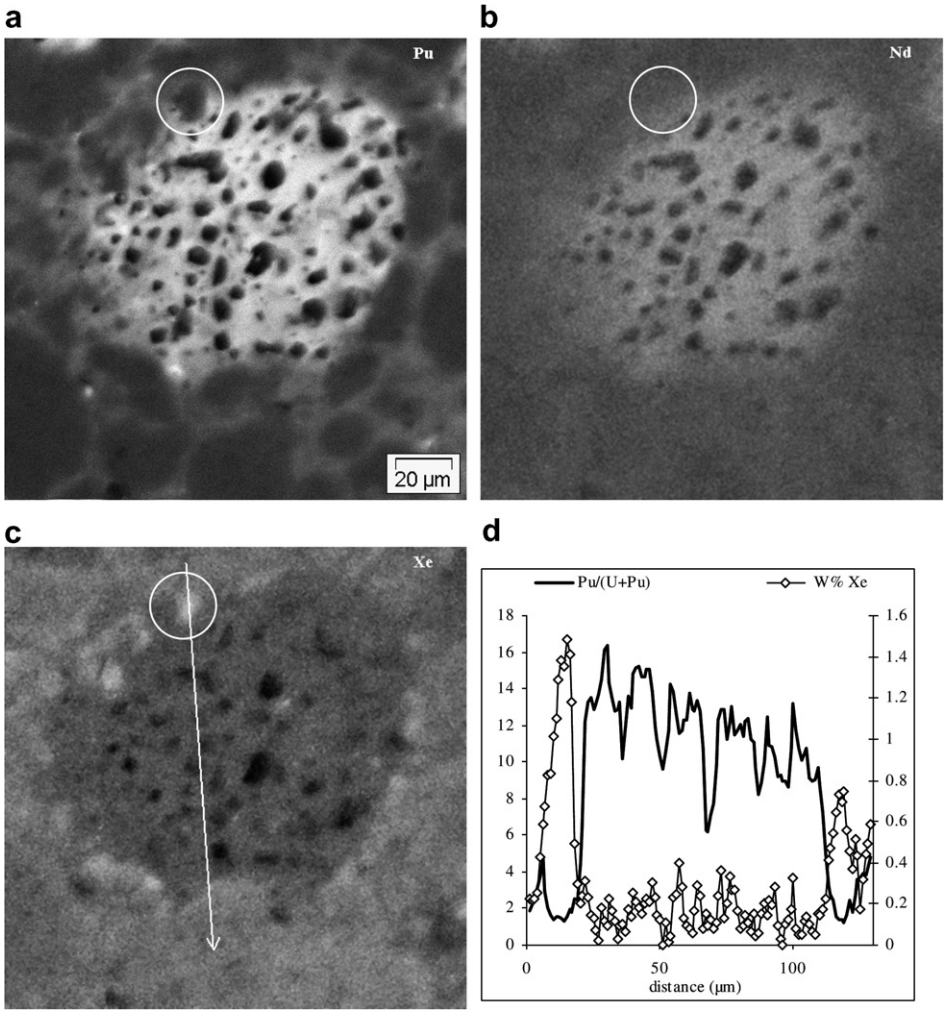

Fig. 13. EPMA X-ray map on Pu, Nd and Xe, and quantitative analysis along a line in a (**4**) MOX MIMAS 58 GWd/t fuel. Very high xenon contents were measured in UO_2 grains when they were very close to Pu-rich agglomerates.

– The high stress levels, which certainly had the greatest impact.
– The high enrichment leading to a lower Pu content at a given burn-up, with the local peripheral burn-up being about 70 GWd/t.
– The stainless steel cladding with chemical properties different from those of Zircaloy and a possible impact on oxygen.
– The high fission density rates.

4.2. HBS properties

4.2.1. As-fabricated pores decrease during the formation of HBS

During the formation of the HBS, most of the initial large-size pores disappear. Some of these pores could still be seen, but their number and, most likely, the size of the remnants were greatly reduced. Together with the HBS porosity, Fig. 17 shows the radial profile of the porosity due to pores with equivalent circular diameters (ECD) greater than 3 µm near the periphery of 62 GWd/t UO_2 fuel (**1**). This profile clearly shows this decrease, which was observed in every studied fuel.

However, Fig. 18 shows the existence of residual fabrication pores inside the highly restructured HBS area of this same fuel. The experimental results do not make it possible to confirm whether these remaining pores were initially particularly large or if another singularity prevented their collapse.

4.2.2. Fission gas release from the rim area is generally low

Generally speaking, the overall fission gas release in PWR fuel clearly increases when the mean rod burn-up reaches values close to 40 GWd/t, i.e., while the HBS is forming. The possible role of the HBS in this increase is of great interest. Kinoshita et al. and Mogensen et al. [1,19] concluded that most of the fission gases were retained in the HBS. This is also what our evaluations showed.

4.2.2.1. Isotopic composition of fission gases. The composition of the gas extracted from the UO_2 rods plenums were

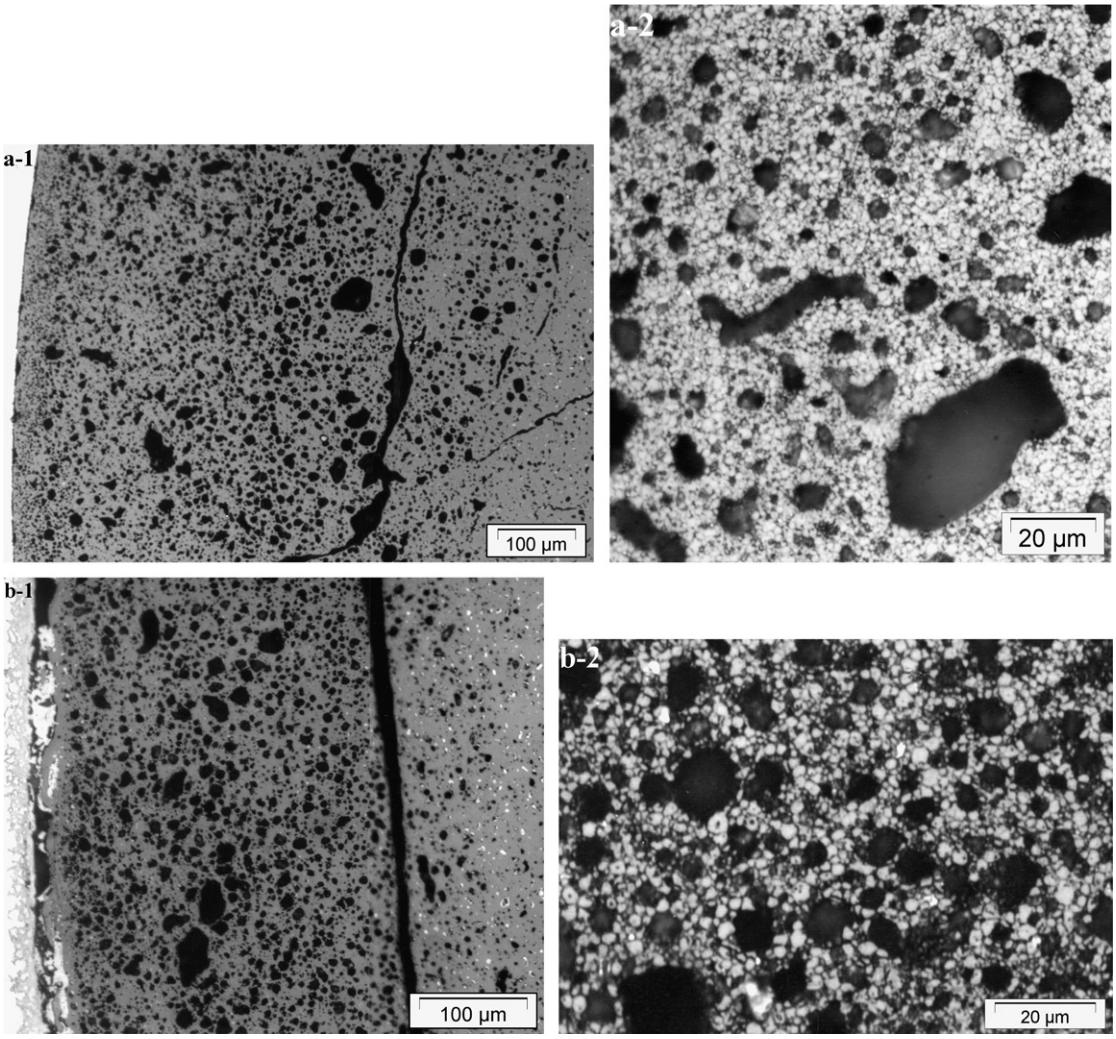

Fig. 14. Optical ceramographs of the periphery of FBR fuels (**6**) at 12.5% FIMA (a) and 17% FIMA (b) before (1) and after (2) chemical etching. The ~10 μm initial grains restructured into smaller grains and large bubbles formed.

measured and the ratios ($^{83}Kr+^{84}Kr)/^{86}Kr$ and ($^{131}Xe+^{132}Xe)/^{134}Xe$ were established as a function of the rods burn-ups (Fig. 19). These ratios increase with the burn-up because of the increasing contribution of plutonium fissions. The higher plutonium content in the rim implies even higher local ratios. The comparison of these ratios with neutron code calculations was presented in [4] for two families of fuels. One was 3.1% ^{235}U-enriched UO_2 fuel irradiated at moderate powers and temperatures. The other fuel family was the UO_2–Zr4 fuel (**2**). In the case of low temperature fuels, a step appears during the formation of the HBS. Our conclusion was that this step was probably the sign of contribution from the rim area to the overall fission gas release, which was low (less than 1.3% at 56 GWd/t). This contribution was evaluated to be about the same as the participation of the knock-out phenomenon and close to one third of the total release. In the case of fuel (**2**), this step was not detected. This does not mean that such releases did not exist at all, but the higher releases observed in these fuels cannot be attributed to the rim participation.

The higher releases were mainly linked to the high temperature in the central area, with the rim participation remaining low so that its impact on the isotopic composition of the released gas was negligible. This method applied to UO_2–M5™ fuels (**3**) reaching burn-ups higher than those in the first study, proves to be very consistent with the results of fuels (**2**) (Fig. 19). It confirms the main result of [4], but does not make it possible to specify the highest release possible in the rim area.

4.2.2.2. SIMS gas measurements. SIMS gas measurements in nuclear fuels were given in [25,26]. During these measurements, local depth profiles of the xenon signal were acquired. In these profiles, two components can be separated: a base line and peaks. The base line results from the solid solution gas and from the gas in bubbles that are so small that their content cannot be distinguished from

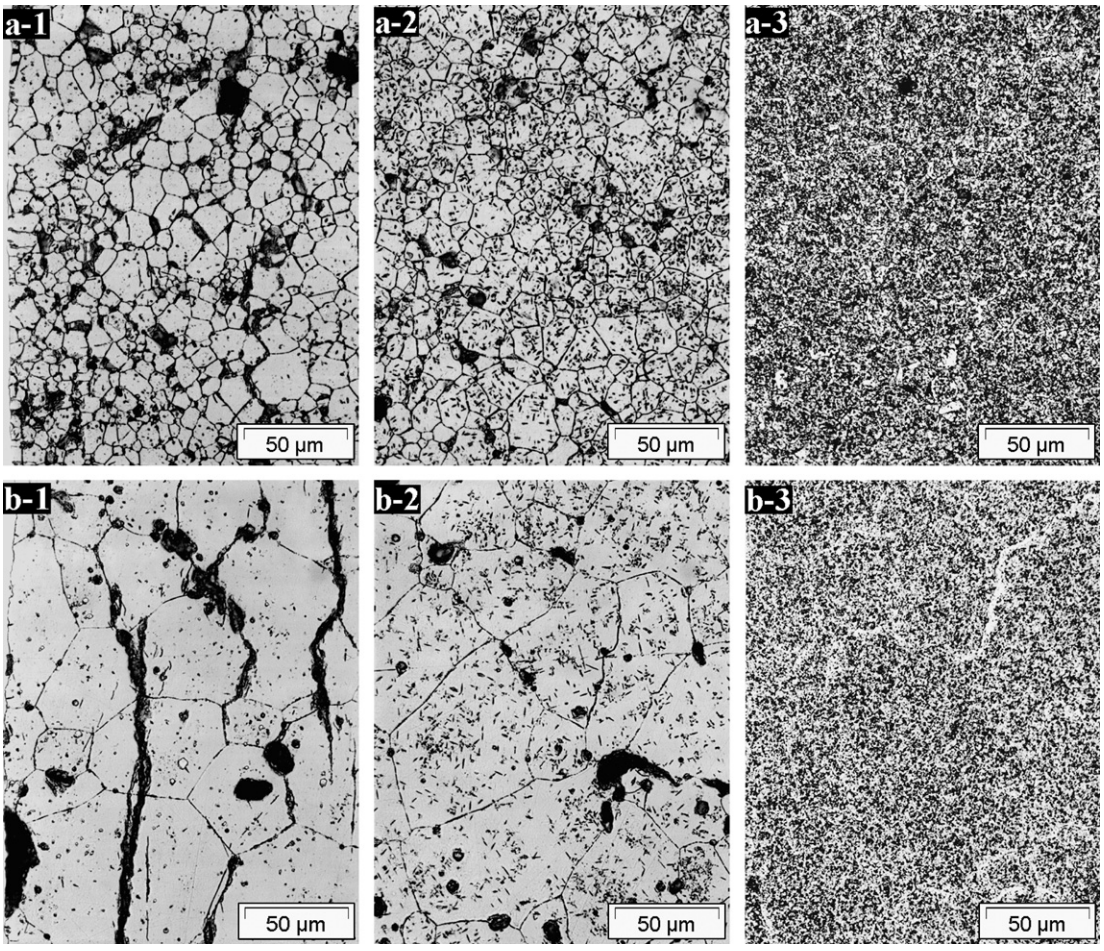

Fig. 15. Optical ceramography after chemical etching of standard (a) and large-grain doped (b) UO_2 fuel from the Tanoxos (**5**) programme at 1R (1) 0.5R (2) and around 0R (3).

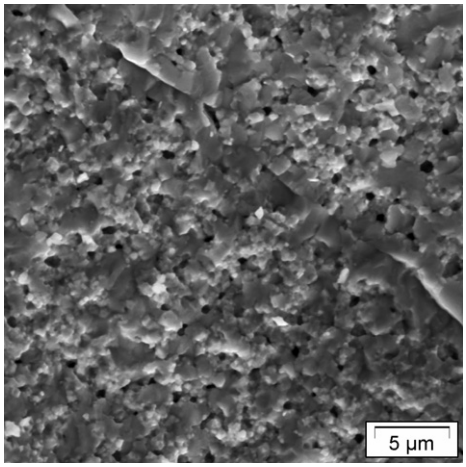

Fig. 16. SEM fractography of the central part of a Tanoxos (**5**) large-grain doped fuel.

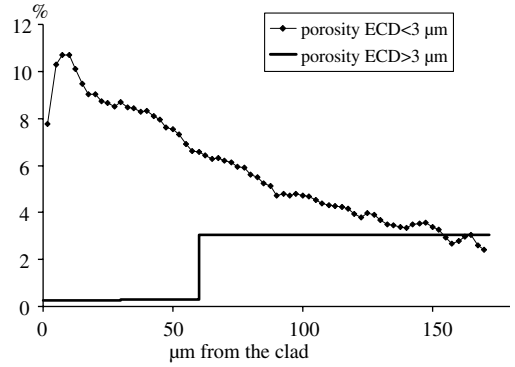

Fig. 17. Peripheral porosity profiles of a (**1**) UO_2–Zr4 fuel at 62 GWd/t mean sample burn-up, with a separation between the <3 μm bubbles and the >3 μm pores.

the baseline noise. It was therefore possible to establish the total signal radial profile and the baseline radial profile from the different depth profiles. Examples were given in [6,26].

Fig. 20 shows such SIMS measurements on the periphery of (**1**) UO_2–Zr4 fuel at 62 GWd/t. Close to the periphery (r/R close to 1), depth profiles show a low baseline level but many bubbles. At $r/R = 0.85$, shows a higher baseline level and only a few bubbles with a lower gas content.

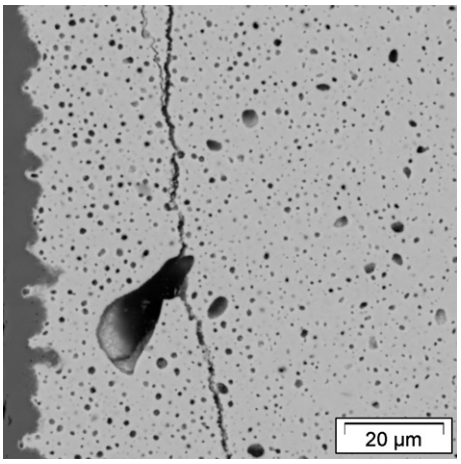

Fig. 18. SEM image of the periphery of a (**1**) UO_2–Zr4 fuel at 62 GWd/t mean sample burn-up, showing a large pore in the HBS rim.

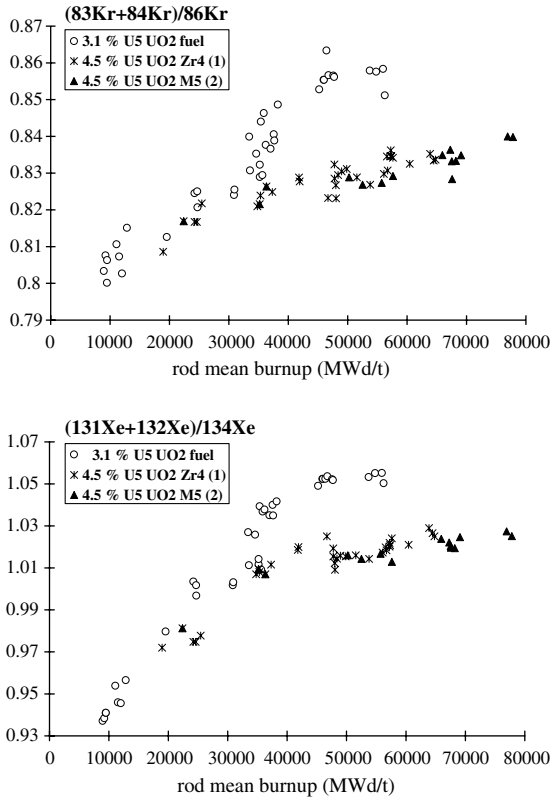

Fig. 19. ($^{83}Kr + {}^{84}Kr$)/^{86}Kr and ($^{131}Xe + {}^{132}Xe$)/^{134}Xe ratios as a function of the mean rod burn-up in the gas extracted from the free volumes of the rods during gas puncturing, for 3 UO_2 PWR types of irradiation.

The deduced radial profile confirms the previous results that most of the gas generated in the rim area remains in the pellets.

This measurement method is still being improved and uncertainties are still too high to precisely specify the amount of gas released from the HBS area during irradiation. The main problem due to the lack of precise knowledge of the volume analysed will soon be solved.

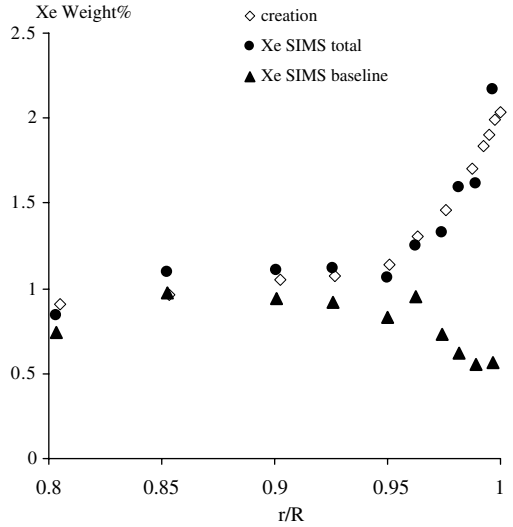

Fig. 20. SIMS xenon measurements on the periphery of a (**1**) UO_2–Zr4 fuel at 62 GWd/t, showing that the xenon content in the HBS is very close from its formation.

4.2.3. The HBS bubbles are highly pressurised

A few independent evaluations lead to the conclusion that HBS bubbles are highly pressurised. The first of these evaluations consists in using the total HBS porosity measured by SEM with the xenon EPMA measurements. This method was first applied to UO_2–Zr4 (**2**) – as exposed in [3] – before being applied to other fuels including MOX fuel. The aim of this evaluation is to obtain an underestimation of the amount of gas inside the HBS bubbles by systematically over-estimating all parameters resulting in a low pressure:

- Over-estimation of HBS local release at 10% of the formed gases (twice the evaluated maximum release in the UO_2 periphery, cf. [4] and Section 4.2.2).
- Explaining the quantity measured by EPMA in these areas by the solid solution xenon, though part of it may have resulted from unopened bubbles under the sample surface.
- Use of the maximum measured porosity.

Considering that krypton behaves similarly to xenon, it was possible to assume that all unreleased gas not measured by EPMA remained in the HBS bubbles, i.e., in a known volume equivalent to the measured porosity. Therefore, the molar volume could be known.

Table 2 and Fig. 21 show the results of this evaluation performed on some of the fuels. The results are always of the same order of magnitude, with a molar volume of about 11×10^{-5} m^3/mol (~180 Å^3/at, i.e., a few times the volume of the UO_2 trivacancy). The pressures in the bubbles were much higher than the expected pressure generated by local stresses and the surface tension forces for these bubble sizes. The molar volume seems to slightly increase with the burn-up, especially in the mid-radius MOX agglomerates.

Table 2
Rough evaluation of the pressure in HBS bubbles at the end of life of various fuels

Fuel type	HBS local burn-up (GWd/t)	Position	Gas volume		Pressure with the Van der Waals equation of state (MPa)
			(m^3/mol)	(Å^3/at)	
(2)	105	Rim	9×10^{-5}	150	90 (at 650 K)
(1)	120	Rim	10×10^{-5}	170	70 (at 650 K)
(3)	120	Rim	9×10^{-5}	150	90 (at 650 K)
(4)	100	Peripheral agglomerate	11×10^{-5}	185	55 (at 650 K)
	80	Mid-radius agglomerate	9×10^{-5}	150	145 (at 900 K)
(4)	160	Peripheral agglomerate	11×10^{-5}	185	55 (at 650 K)
	120	Mid-radius agglomerate	12×10^{-5}	200	80 (at 900 K)
(4)	180	Peripheral agglomerate	10.5×10^{-5}	175	65 (at 650 K)
	130	Mid-radius agglomerate	10.5×10^{-5}	175	105 (at 900 K)
(4)	200	Peripheral agglomerate	11×10^{-5}	185	55 (at 650 K)
	160	Mid-radius agglomerate	12×10^{-5}	190	95 (at 900 K)
(4)	220	Peripheral agglomerate	10×10^{-5}	170	65 (at 650 K)
	150	Mid-radius agglomerate	16×10^{-5}	270	50 (at 900 K)
(4)	270	Peripheral agglomerate	13×10^{-5}	210	45 (at 650 K)
	180	Mid-radius agglomerate	16×10^{-5}	265	55 (at 900 K)

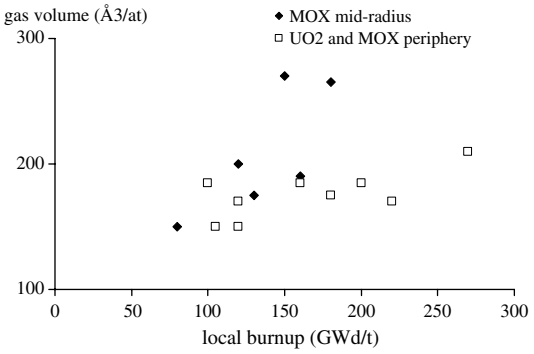

Fig. 21. Atomic volume according to the radial position (extract from Table 2).

Such evaluations are not possible for FBR fuel due to the very high fission gas releases in the pins.

The second evaluation was discussed in [5] and is extended here to the MOX fuel. It is based on the amount of gas measured by SIMS at the opening of a single bubble – by itself an interesting result – associated with the bubble volume as observed by SEM. The results given by this method of evaluation are quite consistent with the previous results.

The amount of gas in one single bubble from the rim area of a UO_2–M5™ (**3**) fuel (61 GWd/t) was found to be about 3×10^{-14} g of xenon in a 0.4 μm diameter bubble. The molar volume was therefore about 13×10^{-5} m^3/mol. The amount of gas in one bubble proved to be much greater in MOX fuel, with a higher local burn-up. In a 63 GWd/t sample peripheral agglomerate from a MIMAS MOX fuel (**4**), in a ~250 GWd/t agglomerate, the amount of gas in one bubble varied from below 10^{-12} g to about 1.5×10^{-10} g, in bubble sizes ranging between 1 μm and 8 μm in diameter. As expected, the range of molar volumes was equivalent to about 10^{-4} m^3/mol.

Our last evaluation is based on the fact that in areas where the HBS had not finished forming (like in the internal part of the rim area), xenon EPMA X-ray maps exhibit zones where the xenon is well measured and others where the measured level is very low. Superposition of the same areas with SEM images show that the zones with high levels of xenon exhibit in fact no bubbles on their surface. However, bubbles detected with the SEM are located in the middle of the xenon low level zones. It is therefore possible to estimate the volume having contained the gas forming the bubbles. Having determined the proportion of local fission gas missing in this volume by quantitative measurements, another estimate of the amount of gas in these bubbles is obtained.

For a 69 GWd/t (**3**) UO_2–M5™ fuel on the limit of the rim area, Fig. 22 shows a xenon X-ray map superimposed

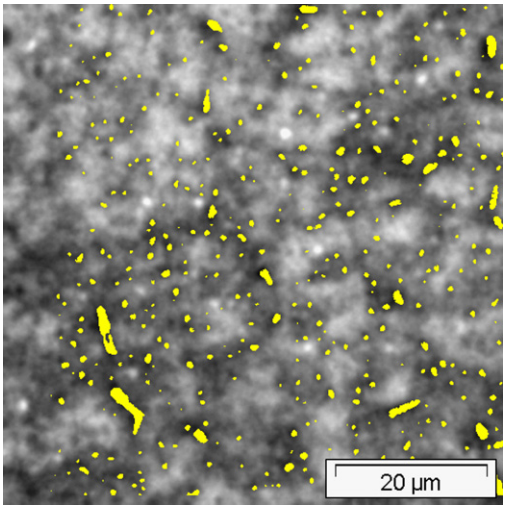

Fig. 22. Superposition of the bubbles cut by the polished surface, as detected by SEM, with the xenon EPMA X-ray map in a 69 GWd/t (**3**) UO_2–M5™ fuel at the limit of the rim area. The visible bubbles are in the middle of the xenon depleted areas.

on a SEM image of the bubbles (in yellow).[1] A volume of about 2 μm in diameter surrounds these bubbles with a diameter of about 0.8 μm. The lack in xenon + krypton in this volume is evaluated at 0.9 wt%. The amount of gas in one bubble is consequently about 4×10^{-13} g, which means that the molar volume is about 9×10^{-5} m^3/mol. This estimation is far less precise than the two previous ones, mainly because the evaluation of the volume is similar to the resolution of the EPMA. Furthermore, it can only be applied in areas where the HBS is not yet fully developed. It nevertheless proved to be quite consistent with the previous results. It must be noted however that EPMA xenon depletion is a direct consequence of the formation of bubbles, with the surface bubbles being opened by the sample preparation. Furthermore, xenon depletion does not occur before the formation of bubbles [27].

4.2.4. Formation of metallic precipitates

During the formation of the HBS, optical micrographs and EPMA X-ray maps clearly show the formation of small metallic precipitates like those found in the hot central areas. In UO_2 fuels, the composition of these precipitates seems to remain close to the formations, but their small size makes it difficult to obtain good EPMA measurements. In MOX fuels where the burn-up in the Pu-rich agglomerates can be higher than it is the UO_2 rim areas, a partial lack of molybdenum from the HBS peripheral precipitates was measured together with an increase of the molybdenum content for the rest of the agglomerate. This evolution is more or less pronounced from one fuel to another with no clear reason for such differences. It can be observed in fuels as soon as the HBS has formed.

4.3. HBS changes with irradiation

4.3.1. UO_2 rim area

Examination of the periphery in the considered UO_2 fuels (**1**), (**2**) and (**3**) shows a practically linear increase of the porosity with the fission product content for any given fuel in the HBS area. This increase in porosity represents both an increase in the number of bubbles, with completion of the restructuring (i.e., the progressive decrease in the unrestructured parts), and an increase in the bubble size firstly due to the accumulation of newly formed fission gases in the already formed bubbles.

For UO_2–Zr4 at 61 GWd/t fuel (**2**), Fig. 23 shows both the decrease in the fission product concentration and the decrease in the porosity close to the cladding.

Fig. 24 gives the radial evolution for the number of bubbles per mm^2 and for the surface density of the rim bubbles in a UO_2–Zr4 fuel **(2)** at 61 GWd/t. For a given UO_2 sample, the decrease in the porosity in relation to the distance

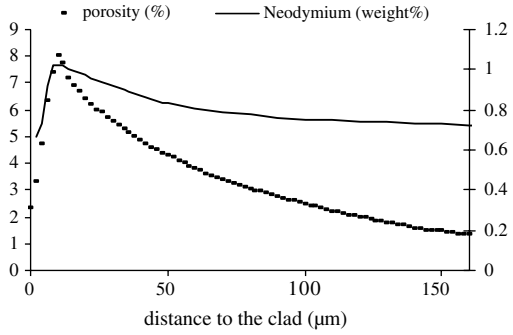

Fig. 23. EPMA neodymium profile and SEM porosity measurement on a 61 GWd/t(**2**) UO_2–Zr4 fuel. The lower porosities at the extreme periphery are due to the lower fission product content as a consequence of the clad implantation.

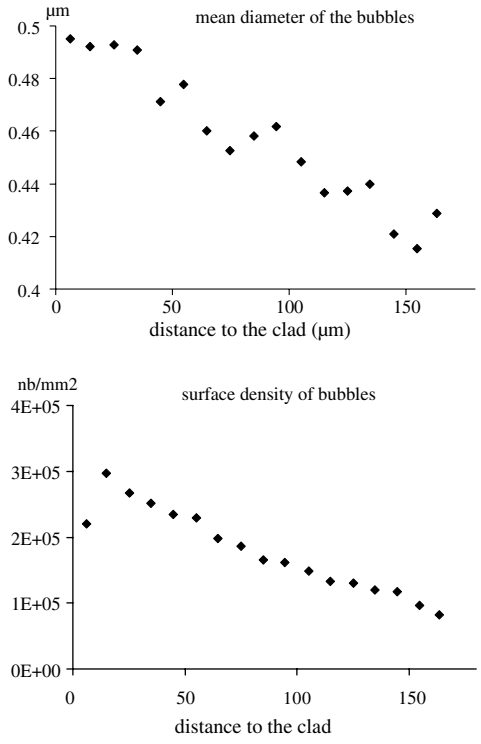

Fig. 24. Radial evolution of the bubble sizes and densities on the periphery of a 61 GWd/t (**2**) UO_2–Zr4 fuel.

to the cladding, i.e., with the decrease in the local fission product content, represents a decrease in the number of bubbles and in their mean size. In this example, the density evolution has more than twice the effect on the total porosity than the evolution in the bubble size.

The increase in the porosity in relation to the increase in the fission product content was the same for all examined fuels (Fig. 25), only its starting point changes. This change reveals the influence of parameters other than the local fission product content. The delay in the formation of the HBS in (**3**) fuels may be explained by the mechanical

[1] For interpretation of color in Fig. 22, the reader is referred to the web version of this article.

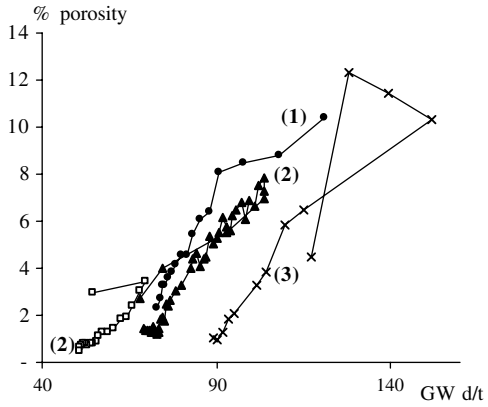

Fig. 25. Evolution in the local HBS porosity as a function of the local burn-up (deduced from the neodymium content) for samples of (**1**), (**2**) and (**3**) UO_2 fuels.

properties of the M5™ cladding which induce higher stress in the fuel once the gap is closed.

With the increase in burn-up, inter-penetration is observed between the HBS rim and the zirconia formed at the cladding inner surface after closure of the pellet-to-cladding gap (Fig. 26 for a (**2**) UO_2–Zr4 fuel with a local burn-up of 69 GWd/t). Some small fission gas bubbles are also observed in the zirconia, particularly in the parts having penetrated the HBS. This phenomenon illustrates the deformation capacities of the HBS. Moreover, the bonding between the pellets and the clad is very strong. This strong bonding and the differential thermal expansion of the pellet and cladding lead to circumferential cracks in the HBS during the cooling phases. Some of these cracks can be seen crossing previously formed HBS bubbles in Figs. 26 and 18. This is a HBS fission gas release mechanism that has to be taken into account though its impact remains to be evaluated.

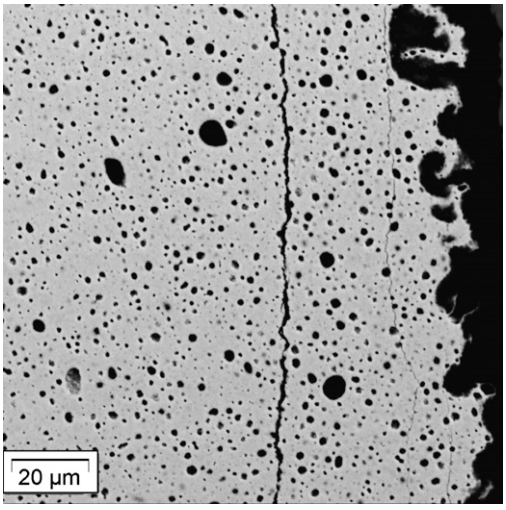

Fig. 26. 69 GWd/t(**2**) UO_2–Zr4 sample, rim and zirconia interpenetration increase at high burn-up, formation of peripheral cracks in the HBS.

4.3.2. MOX fuel plutonium agglomerates

Examination of plutonium-rich agglomerates makes it possible to observe the changes in the HBS at much higher burn-ups. The agglomerates on the periphery showed:

- No major evolution in the sub-grain sizes after formation.
- A continuous increase in the porosity in relation to the burn-up.
- An increase in the bubble size and a decrease in their number as the burn-up increases.

These variations not only result from the continuous arrival of fission gases in the previously formed bubbles, but also from the coalescence of these bubbles at very high burn-up, as seen in Figs. 27 and 28. The images (Fig. 27) of mid-radius agglomerates and (Fig. 28) in a peripheral agglomerate show the role of the local deformations that are necessary to obtain, first the coalescence and then big-

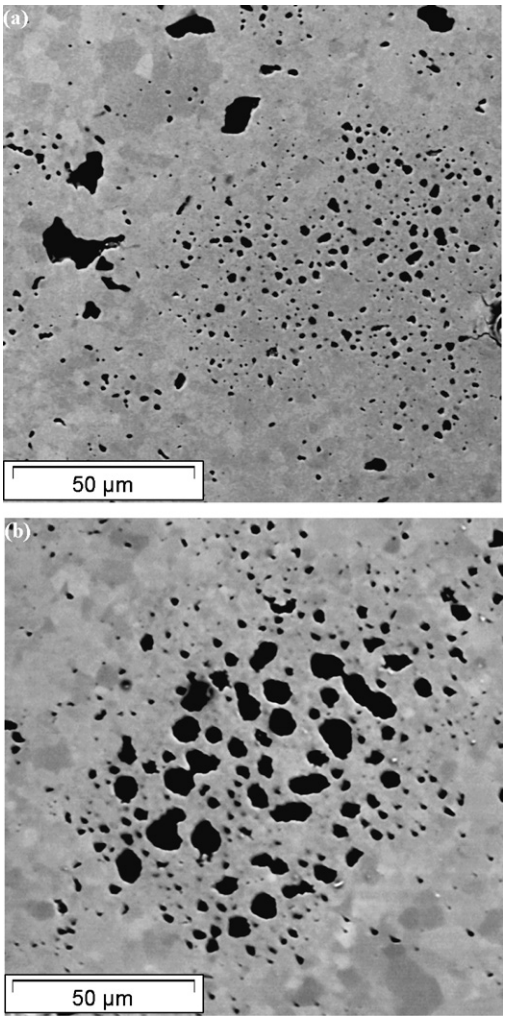

Fig. 27. Increase in the size of HBS bubbles in the mid-radius agglomerates of (**4**) MIMAS MOX with (a) 100 GWd/t and (b) 150 GWd/t burn-up in the agglomerates.

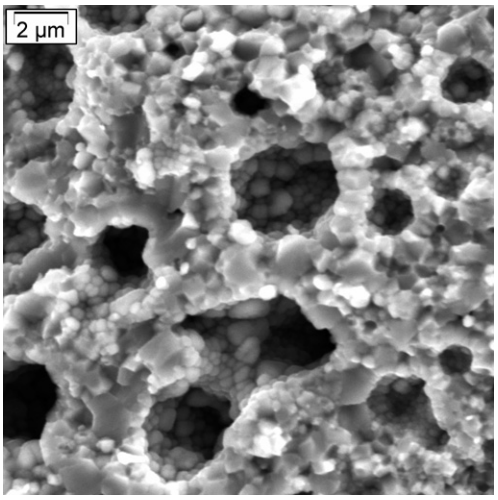

Fig. 28. HBS of a MOX Pu-rich agglomerate **(4)** in which the burn-up was about 180 GWd/t. Coalescence of the bubbles and round sub-grains surrounding these bubbles.

ger bubbles with general shapes that are usually almost spherical.

Fig. 29 shows the structure of one of the maximum burn-ups observed on the periphery of a (**4**) MOX fuel in which the local burn-up in the Pu-rich agglomerate was around 270 GWd/t. In these agglomerates, in spite of the low temperature, the equivalent circular diameter (ECD) of the HBS bubbles was capable of exceeding 10 μm, whereas the surrounding HBS bubbles remained below 2 μm.

Fig. 30 shows the progressive increase in the total porosity of the centre of the peripheral and the mid-radius Pu-rich agglomerates. This graph provides more or less the same information as that given in Table 2, as these porosity measurements were used to evaluate the molar volume of the fission gases in the bubbles. When comparing MOX

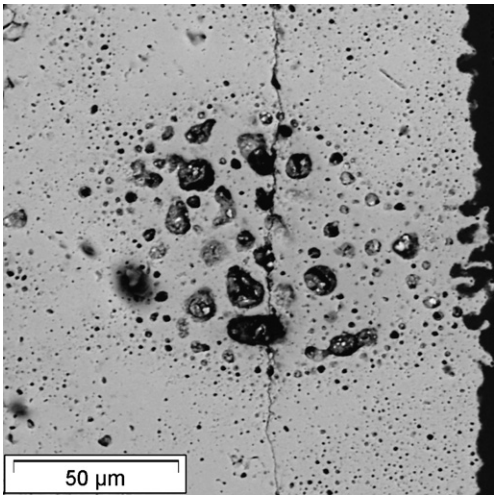

Fig. 29. One of the maximum local burn-up observed in a peripheral agglomerate of a PWR MOX MIMAS (**4**) fuel. The local burn-up was about 270 GWd/t and some bubbles were larger than 10 μm in diameter.

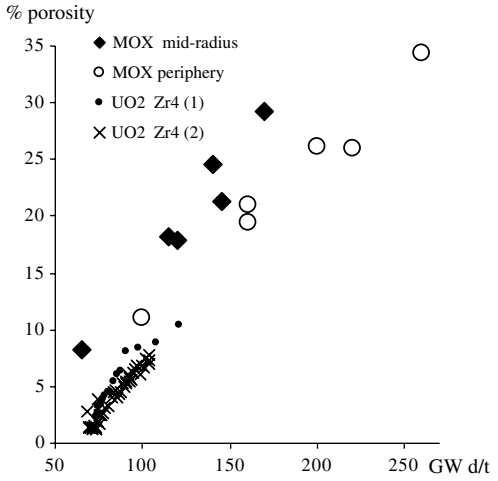

Fig. 30. Increase of the porosity in the centre of large Pu-rich agglomerates in relation to the local burn-up for MOX fuel. This porosity is slightly higher than the UO_2 porosity, but its increase is similar in the peripheral agglomerates. The mid-radius agglomerates show an even higher porosity.

and UO_2 peripheries, the porosity tends to be slightly larger in the MOX agglomerates, though its increase at very high burn-up remains rather consistent with what is seen in the UO_2 rim at lower burn-ups This increase in porosity is more than twice the standard overall fuel swelling (~0.6%/10 GWd/t), which surprisingly was also the porosity increase rate measured in [28] for very high burn-up UO_2 fuels. The porosity in the mid-radius agglomerates seems to increase at a slightly faster rate (an increase in the molar volume can be observed in Table 2).

Fig. 31 shows the bubble sizes in the centre of the MOX (**4**) peripheral agglomerates. It clearly shows the increase in the size of these bubbles and, with the appearance of very large bubbles by coalescence, the formation of bubbles more than twice the volume of the other large bubbles. Still, it is rather unclear whether the decrease in the amount of bubbles only results from this coalescence or if ripening should be taken into account as recommended in [28].

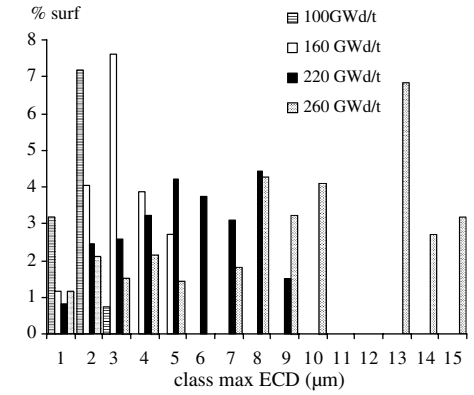

Fig. 31. Changes in the bubble sizes in the centre of the large peripheral Pu agglomerates in relation to the burn-up in MOX (**4**) fuels.

Such ripening would imply resolution, by the fission spikes, of fission gas atoms, from rather large (more than 1 μm) and highly pressurised bubbles with a high diffusion of these gases in the grains or at the grain boundaries. We have no evidence in favour of such a phenomenon, but we cannot be sure that the bubble growth owing to the newly generated gas and eventually by coalescence suffices to explain such observations.

It must be pointed out that no new major phenomenon was detectable, even at such very high burn-ups.

Effects of the HBS behaviour (over-pressurisation of bubbles, coalescence, specific mechanical properties) are felt when the stress context differs from the fuel-to-clad interface conditions or the usual conditions in MOX agglomerates. Fig. 32 shows an example of a MIMAS MOX fuel **(4)** in which a plutonium-rich agglomerate happened to be at the pellet surface on a chamfer. Optical microscopy on a longitudinal cut revealed the high swelling in this agglomerate, without fuel dispersion in the chamfer. The porosity measured in this agglomerate was about 50%. Such swelling and deformation properties (see [29]) certainly explains the decrease in the fabrication porosity in UO_2 rim areas.

Lastly, in the MOX Pu-rich agglomerates, a mobility of cesium was measured. This mobility was pronounced in the hot central parts of the pellets, and also exists in the extreme periphery. Fig. 33 shows the EPMA measured ratio between cesium and neodymium in the grains of large MOX agglomerates on the periphery of increasing burn-up MOX fuels. The mobility of cesium increases with the local burn-up despite the very low temperatures during irradiation. Some of this cesium can be found in the agglomerate HBS bubbles.

4.3.3. Amount of gas in the HBS grains

In all highly developed HBS, the EPMA always detects a small amount of xenon. Fig. 34 gathers the mean results

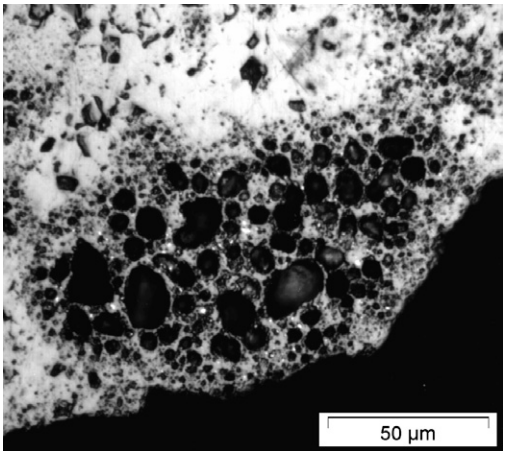

Fig. 32. Optical ceramography of a 52 GWd/t sample of MOX **(4)** in which an agglomerate was located on the chamfer (longitudinal cut). Visualisation of swelling in the agglomerate.

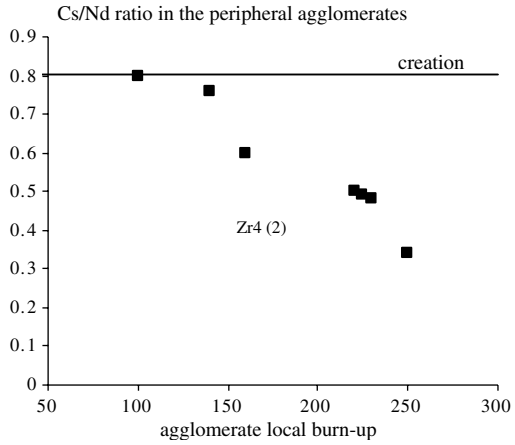

Fig. 33. Cesium/neodymium ratio decrease in relation to the burn-up in the peripheral agglomerates of MOX fuels.

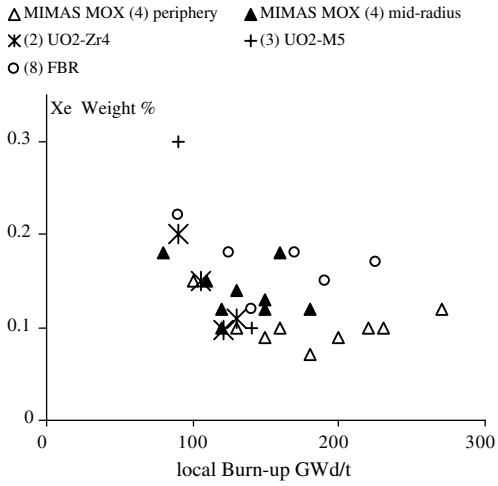

Fig. 34. EPMA xenon measurements in HBS from various fuels as a function of the local burn-up.

obtained for various HBS, given as a function of the local burn-up at the measurement positions.

From Fig. 34, it first seems that there is a slight general decrease on the amount of gas retained in the grains. This decrease may be partially artificial as, in the EPMA measurement at low burn-up, part of the signal may come from sub-micronic bubbles still full of gas under the polished surface. Statistically, this participation tends to decrease when the bubble size increases [30]. It is therefore possible that the lowest burn-up values be slightly over-evaluated. Nevertheless, it is reasonable to think that a slight decrease exists. In the HBS of UO_2 fuels and PWR MOX fuels in the peripheral agglomerates, i.e., in a family of HBS that underwent similar irradiation temperatures, and in spite of the differences of the sub-grains sizes (a bit larger in the MOX cases), the measurement are rather close for a given burn-up. They start around 0.2 wt% and reach rapidly values lower than 0.1 wt% of xenon. This value should be taken into account for modelling [31]. Slightly higher values are measured in the mid-radius MOX agglomerates

and in the FBR fuels, with larger sub-grains and higher irradiation temperatures. Nevertheless, the measurements are soon lower than 0.2 wt%.

5. Discussion

5.1. Main results for discussion

- *Formation of planar defects*:
  Prior to the formation of bubbles and sub-grains, planar defects appear as intragranular disks with a diameter of ~1 μm exhibiting free surfaces. Round sub-grains form on these surfaces and the planar defects change into bubbles. In highly developed HBS, planar defects are no longer observed.
- *Chemical effects and evolutions*:
  The formation of the HBS is influenced by the chemical composition of the high burn-up fuel. In particular, the amount of plutonium seems to have an impact. This result explains one of the questions arising in the conclusion of [27] in which a delay in the rim porosity growth was reported in the case of high ^{235}U enrichments. In this case, the plutonium formation at a given burn-up is lower. This leads us to suggest that, apart from the elements added during fabrication, the trivalent fission products have an effect on the formation of the HBS. These elements, together with the plutonium content, are the main contributors to the oxygen potential increase during irradiation both in PWR fuel [32] and in FBR fuel in which the HBS and the JOG form at the same time. Though less pronounced in PWR fuels than in FBR fuels, the formation of the HBS was also related to chemical evolutions in the metallic fission products and the volatile elements such as cesium. The partial departure of molybdenum from the metallic precipitates in the plutonium agglomerates of MOX fuels must be regarded as a chemical effect linked to the formation of the HBS. The TEM observations in [15] show that molybdenum depletion also occurred in UO_2, with the missing molybdenum having been precipitated in an unidentified phase associated with the HBS bubbles. Furthermore, an oxide deposit near the external surface of the pellet (with Cs, Ba, Zr, Te, I and Ag) was also reported and may be a phenomenon similar to the JOG and the cesium movements observed in the MOX.
- *The highly pressurised bubbles*:
  The molar volume in the peripheral bubbles of the rim area or in the HBS of the agglomerates was always about 10^{-4} m^3/mol. This is much lower than the equilibrium value for these bubbles. This conclusion is quite consistent with conclusions in [33], though this document reports higher molar volumes. In the hottest HBS areas, i.e., the mid-radius MOX plutonium-rich agglomerates, the molar volumes increased slightly with the burn-up, which is sign of progression towards equilibrium. Nevertheless, even then, equilibrium was far from being reached.
- The initial grain boundaries do not usually play a significant role in initiating the HBS.
- High levels of deformation in HBS materials are found.

This was observed in the case of an HBS on the surface of the chamfers, at the interface with internal zirconia, in the decrease of the initial pores, and in the coalescence of bubbles at very high burn-up.

5.1.1. Comparison with the main theories

Attempts to explain the formation of the HBS fall into three main categories:

(1) In [34,35], the accumulation of irradiation damage in high burn-up areas is considered to lead to inhomogeneous accumulations of dislocations, so that a tangled dislocation network becomes organised into subdivided grains with high angle boundaries. These grains are nuclei for grain growth (recrystallisation). It then seems that the fission gases are swept out of these new grains during their growth to form bubbles.

(2) Paper [36] – with additional information in [37] – suggests considering that the accumulation of radiation damage leads to a dislocation network in which polygonisation occurs, forming low angle boundaries with small divided grains. In [37], polygonisation starts when the accumulation of rare gases and metallic fission products results in enough precipitates to anchor the dislocations. Some gaseous and metallic fission products can then form larger bubbles and precipitates by moving in correlation with vacancies in the sub-grain boundaries, thus promoting the rotation of newly formed small grains.

These two explanations are based on the same reasoning, which is the accumulation of radiation damage and the formation of dislocations. The debate on the angle boundaries between the newly formed grains is based on different measurements among the various teams working with TEM. The grain growth process of (1) is contested in this second case in which a division of the initial grains is considered as being more consistent with the HBRP (high burn-up rim project) examinations.

(3) In [33,27], it was suggested that some recrystallisation could be localised around the formed fission gas bubbles by a local build up of the mechanical stresses induced by the high pressure in these bubbles. The possibility of recrystallisation or polygonisation prior to the formation of the bubbles was considered as inconsistent with the experimental observations.

Comparison of these three explanations with our new experimental data rises a few problems:

- The existence of planar defects was not considered in these theories. Moreover, these defects cannot be explained by the formation and accumulation of dislocations.
- The possible chemical effects of plutonium do not seem to have any explanation.

– The evolution of cesium and molybdenum was not taken into account.
– In the two first proposals, over-pressurisation in the HBS bubbles is difficult to understand as they both imply an evolution in the system towards equilibrium.
– The two first proposals assert that the grain boundaries play a special role in the initiation of the HBS. They also consider recrystallisation or polygonisation prior to the formation of the bubbles. This is contested by both the third proposal and our own results.

5.1.2. Proposal of two new mechanisms

Very local (μm range) traction stresses are necessary for the formation of planar defects. These stresses cannot come from the over-pressurised bubbles since planar defects appear before the formation of bubbles. Our hypothesis is that these local stresses are due to a local evolution in the crystal structure. A major observation was reported in [38] Fig. 2 detail B. In this detail of a high burn-up UO_2 fuel, the lattice image obtained from the [1 1 0] direction exhibits an area where the lines seem to gather two by two to form a larger line. The diffraction pattern in this area suggests that this is a micro-domain of an over-structure of the UO_2. It is likely that the high content of fission products in solid solution in the bulk of the oxide in the high burn-up areas, as well as the presence of Pu, locally lead to the formation of an over-structure with a lower lattice parameter [39]. The first mechanism that we propose is that the formation of this over-structure results in planar defects. Recently, Kinoshita et al. [40] suggested an alternative explanation in which the planar defects would be oxygen defects on [1 1 1] crystallographic planes.

Secondly, once a planar defect is formed, its surfaces are free surfaces subjected to fission spike solicitations. These free surfaces are then modified just like the pellet free surfaces (large initial pores – Fig. 35, cracks, dishings, etc.).

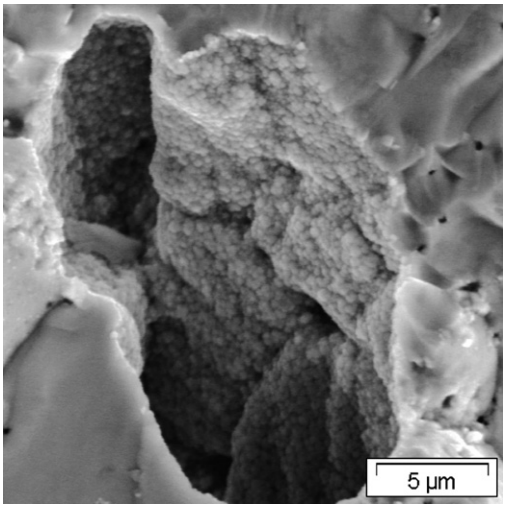

Fig. 35. Round sub-grains formed on the surface of a large as-sintered pore of a UO_2–M5™ (**3**) 73 GWd/t pellet.

This phenomenon is similar to what is observed on the surface in the case of ion bombardments [41] and what is also seen in the case of ion plating [42]. Both lead to larger ripples or larger grains for higher temperatures. During this surface modification leading to the formation of sub-grains, some of the fission products are trapped in the formed volume, and the bubbles form, with a deformation in the shape of the planar defects, towards a practically spherical shape observed in the HBS areas. The bubble formation process must be rather fast once the surface deformation has started, as only a few planar defects are found in an intermediate state. This mechanism would explain the high pressure in the bubbles and the slow growth of the bubble volume following their formation, with the same phenomenon causing the bubbles to be filled with gas and to deform. In the MOX mid-radius agglomerates, the increase in the molar volumes probably implies a higher vacancy flux.

Based on these hypotheses, the very initiation of the HBS would mainly result from the solid solution of atoms such as the trivalent rare earths and the plutonium, rather than the gases, or the metallic or volatile fission products. Nevertheless, its subsequent changes with the formation of bubbles imply these other fission products.

6. Conclusion

A selection of high burn-up structure examinations on a wide variety of fuels was used in this paper to answer to some of the questions concerning the formation of HBS and its subsequent changes.

It was shown that:

– The HBS has high fission gas retention capacities. In particular, the HBS does not evolve towards an open system of interconnected channels, even when porosity reaches very high values (35% in a FBR fuel, 50% in a PWR MOX unstressed agglomerate). Our experience is therefore consistent with [43]. Furthermore, HBS bubbles are over-pressurised in most cases.
– After a stage of initiation and spreading of the HBS, the bubbles grow, being fed with newly formed gas atoms, while coalescence is observed, leading to a decrease in the number of bubbles while their size increase. We have no element showing that this coalescence is the only phenomenon leading to the decrease in the number of bubbles.
– The presence of plutonium may have an effect on the initiation of the HBS. This point should be checked by dedicated experiments designed to avoid all other possible influences (temperature, high stress, flux rate differences).
– The stress level seems to have an impact on the formation of HBS.
– The size of the newly formed grains increases with the irradiation temperature, as does the size of the formed

bubbles. However, the grain sizes do not undergo any further major evolution afterwards.
- The initial grain boundaries are usually not essential in the initiation of HBS.
- The initial fabrication pores are greatly reduced during the formation of HBS.
- The increasing interpenetration between the HBS and the internal zirconia leads to the formation, of peripheral cracks in the UO_2 rim areas during the cooling steps, inducing fission gas release.
- The increase in porosity in the HBS occurs at similar rates both in UO_2 fuels and in the centre of the large peripheral MOX agglomerates, in which porosities of more than 30% can be observed.
- Planar defects (1) first appear during the HBS formation process, (2) undergo the formation of round sub-grains at their surface, and (3) eventually evolve into bubbles.

Two new mechanisms have therefore been suggested to explain these observations:

- Firstly, the formation of micro-domains of over-structures to explain the formation of planar defects.
- Secondly, fission spikes to explain how the surface changes into round sub-grains and the formed cavities are supplied with fission gases.

Further investigation will nevertheless be necessary using other techniques such as TEM and micro X-ray diffraction, as well as studies on phase formations in the U–O–Lanthanides systems. Confrontation of these ideas with results accumulated by other teams working on this subject will also be required.

Acknowledgements

All fuels discussed in this paper were irradiated and examined within the framework of collaboration between Areva, Electricité de France (EDF) and the CEA. Due to the wide range of techniques and programmes involved, the authors are also indebted to most of the people working in the CEA LECA-STAR hot cell facility at Cadarache.

References

[1] M. Kinoshita, T. Sonoda, S. Kitajima, A. Sasahara, T. Kameyama, T. Mastumura, E. Kolstad, V.V. Rondinella, C. Ronchi, J.P. Hiernaut, T. Wiss, in: International Meeting on LWR Fuel Performance 19–22.09.2004, Orlando, FL (USA) ANS, AESJ, ENS Proceedings of the Conference, 2004, p. 207.
[2] P. Guedeney, M. Trotabas, M. Boschiero, C. Forat, P. Blanpain, in: Proceedings of the International Topical Meeting on LWR Fuel Performance, Avignon, Fr, 1991.
[3] N. Lozano, L. Desgranges, D. Aymes, J.C. Niepce, J. Nucl. Mater. 257 (1998) 78.
[4] J. Noirot, L. Desgranges, P. Marimbeau, in: Fission Gas Behaviour in Water Reactor Fuels, Seminar Proceedings, Cadarache, France, 26–29 September 2000, NEA/OECD, NEA #03053, 2002, p. 223 (ISBN 92-64-19715-X).
[5] J. Lamontagne, J. Noirot, L. Desgranges, Th. Blay, B. Pasquet, I. Roure, Microchim. Acta 145 (2004) 91.
[6] J. Noirot, L. Noirot, L. Desgranges, J. Lamontagne, Th. Blay, B. Pasquet, E. Muller, in: Proceedings of the International Topical Meeting on LWR Fuel Performance, Orlando, USA Fl, 2004, Paper 1019, p. 329.
[7] J. Lamontagne, L. Desgranges, Ch. Valot, J. Noirot, Th. Blay, I. Roure, B. Pasquet, Microchim. Acta 155 (2006).
[8] P. Blanpain, L. Brunel, X. Thibault, M. Trotabas, in: Proceedings of the International Topical Meeting on LWR Fuel Performance, Park City, Utah USA, 2000.
[9] Y. Guérin, J. Noirot, D. Lespiaux, C. Struzik, P. Garcia, P. Blanpain, G. Chaigne, in: Proceedings of the International Topical Meeting on LWR Fuel Performance, Park City, Utah USA, 2000.
[10] L. Caillot, J. Noirot, Y. Pontillon, S. Valin, in: TANOXOS: An Analytical Irradiation Program Aiming at Understanding the Behaviour of Various Doped UO_2 Fuels, TOPFUEL 2006 Salamanca, p. 524.
[11] C. Nonon, J.C. Menard, S. Lansiart, J. Noirot, S. Martin, GM. Decroix, O. Rabouille, C. Delafoy, B. Petitprez, Pellet-clad Interaction in Water Reactor Fuels, 9–11 March 2004, NEA/OECD, NEA#06004, 2005, p. 305, (ISBN 92-64-01157-9).
[12] C. Delafoy, P. Blanpain, S. Lansiart, P. Dehaudt, R. Castelli, in: Proceedings of the IAEA Technical Meeting on Improved Fuel Pellet Materials and Designs, 20–24 October 2003 Brussels, Belgium, IAEA TECDOC1416, 2004, p. 163.
[13] S.R. Pati, A.M. Garde, L.J. Clink, in: Proceedings ANS International Topical Meeting on Fuel Performance, Williamsburg, Virginia, 1988, p. 204.
[14] L.E. Thomas, R.E. Einziger, R.E. Woodley, J. Nucl. Mater. 166 (1989) 243.
[15] L.E. Thomas, C.E. Beyer, L.A. Charlot, J. Nucl. Mater. 188 (1992) 80.
[16] D. Lespiaux, J. Noirot, P. Menut, International Topical Meeting on LWR Fuel Performance, March 2–6, Portland, 1997, p. 650.
[17] Y. Pontillon, M.P. Ferroud-Plattet, D. Parrat, S. Ravel, G. Ducros, C. Struzik, I. Aubrun, G. Eminet, J. Lamontagne, J. Noirot, A. Harrer, in; Proceedings of the International Topical Meeting on LWR Fuel Performance, Orlando, USA Fl, 2004, Paper 1025, p. 490.
[18] K. Une, M. Hirai, K. Nogita, T. Hosokawa, Y. Suzawa, S. Shimizu, Y. Etoh, J. Nucl. Mater. 278 (2000) 54.
[19] M. Mogensen, J.H. Pearce, C.T. Walker, J. Nucl. Mater. 264 (1999) 99.
[20] M. Tourasse, M. Boidron, B. Pasquet, J. Nucl. Mater. 188 (1992) 49.
[21] K. Maeda, T. Asaga, J. Nucl. Mater. 327 (2004) 1.
[22] M. Naganuma, K. Maeda, N. Nakae, J. Rouault, J. Noirot, G. Crittenden, C. Brown, in: Proceedings of 6th International Conference on Nuclear Engineering (ICONE-6) (1998) San Diego, California, USA, 10–15 May, ICONE-6257.
[23] M. Naganuma, J. Noirot, D. Lespiaux, S. Koyama, T. Asaga, J. Rouault, G. Crittenden, C. Brown, IAEA-SM-385/24, 1999, in: Proceedings of International Symposium on MOX Fuel Cycle Technologies for Medium and Long-Term Deployment, Vienna, Austria, 17–21 May 1999, p. 311.
[24] J.C. Dumas, PHD report, Ecole Nationale Supérieure de Physique de Grenoble, Institut National Polytechnique de Grenoble 1995.
[25] L. Desgranges, B. Pasquet, Nucl. Instrum. and Meth. B 215 (2004) 545.
[26] L. Desgranges, J. Nucl. Mater., submitted for publication.
[27] J. Spino, D. Baron, M. Coquerelle, A.D. Stalios, J. Nucl. Mater. 256 (1998) 189.
[28] J. Spino, A.D. Stalios, H. Santa Cruz, D. Baron, J. Nucl. Mater. (2006).
[29] J. Spino, J. Cobos-Sabate, F. Rousseau, J. Nucl. Mater. 322 (2003) 204.
[30] M. Verwerft, J. Nucl. Mater. 282 (2000) 97.
[31] P. Blair, A. Romano, Ch. Hellwig, R. Chawla, J. Nucl. Mater. 350 (2006) 232.

[32] Hj. Matzke, J. Nucl. Mater. 223 (1995) 1.
[33] J. Spino, K. Venix, M. Coquerelle, J. Nucl. Mater. 231 (1996) 179.
[34] L.E. Thomas, C.E. Beyer, L.A. Charlot, J. Nucl. Mater. 188 (1992) 80.
[35] K. Nogita, K. Une, J. Nucl. Mater. 226 (1995) 302.
[36] I.L.F. Ray, Hj. Matzke, H. Thiele, M. Kinoshita, J. Nucl. Mater. 245 (1997) 115.
[37] T. Sonoda, M. Kinoshita, I.L.F. Ray, T. Wiss, H. Thiele, D. Pellottiero, V.V. Rondinella, Hj. Matzke, Nucl. Instrum. and Meth. B 191 (2002) 622.
[38] K. Nogita, K. Une, J. Nucl. Mater. 250 (1997) 244.
[39] J. Spino, D. Papaioannou, J. Nucl. Mater. 281 (2000) 146.
[40] M. Kinoshita, H.Y. Geng, Y. Chen, Y. Kaneta, M. Iwaswa, T. Ohnuma, T. Sonoda, K. Yasugan, S. Matsumura, K. Yasuda, M. Sataka, N. Ishikawa, Y. Chimi, J. Nakamura, M. Amaya, Study of Irradiation Induced Restructuring of High Burnup Fuel – The New Cross-over Project (NXO) to Study RIM-structure Formation, TOPFUEL 2006 Salamanca, p. 248.
[41] U. Valbusa, C. Boragno, F. Buatier de Mongeot, J. Phys. Condens. Matter 14 (2002) 8153.
[42] J.A. Thornton, Annu. Rev. Mater. Sci. 7 (1977) 239.
[43] J. Spino, D. Papaioannou, J.P. Glatz, J. Nucl. Mater. 328 (2004) 67.